Electronic supplementary information

Balancing charge-transfer strength and triplet states for deep-blue thermally activated delayed fluorescence with an unconventional electron rich dibenzothiophene acceptor

Rongjuan Huang,[a] † Nadzeya A. Kukhta,[b] † Jonathan S. Ward,[b] Andrew Danos,[a] Andrei S. Batsanov,[b] Martin R. Bryce,[b]* Fernando B. Dias[a] *

[a]*Department of Physics, Durham University, South Road, Durham, DH1 3LE, UK.*

[b]*Department of Chemistry, Durham University, South Road, Durham, DH1 3LE, UK*

Emails of corresponding authors: f.m.b.dias@durham.ac.uk; m.r.bryce@durham.ac.uk

Contents **Page**

S1. Synthesis and Characterization

S1a. General experimental details

All reactions were carried out under an argon atmosphere unless otherwise stated. Starting materials were purchased commercially and were used as received. Solvents were dried using an Innovative Technology solvent purification system and were stored in ampoules under argon. TLC analysis was carried out using Merck Silica gel 60 F254 TLC plates and spots were visualised using a TLC lamp emitting at 365, or 254 nm. Silica gel column chromatography was performed using silica gel 60 purchased from Sigma Aldrich. ^{1}H and ^{13}C{^{1}H} NMR spectroscopy was carried out on Bruker AV400, Varian VNMRS 500 and 700, and Varian Inova 500 NMR spectrometers. Residual solvent peaks were referenced as described in the literature, [1] and all NMR data was processed in MestReNova V12. Melting points were carried out on a Stuart SMP40 machine with a ramping rate of 4 °C min^{-1}. Videos were replayed manually to accurately determine the melting point. High resolution mass spectrometry was carried out on a Waters LCT Premier XE using ASAP ionization and TOF detection. Samples were analyzed directly as solids using N_2 at 350 °C. Elemental analysis was performed on an Exeter Analytical E-440 machine. TGA analysis was carried out on a Perkin Elmer Pyris 1 machine under nitrogen gas at 20 mL min^{-1}. Measurements were carried out from 25 °C – 500 °C at 10 °C min^{-1}.

S1b. Synthesis and characterization

2,8-Bis(9,9-dimethylacridin-10(9H)-yl)dibenzo[b,d]thiophene (DAc-DBT)

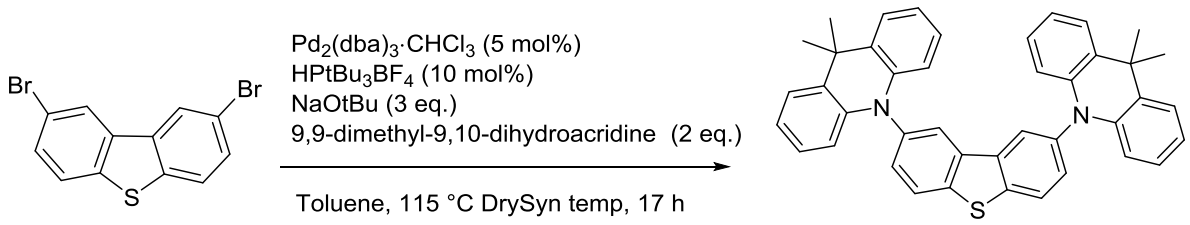

2,8-Dibromodibenzothiophene (268 mg, 0.78 mmol, 1 eq.) and 9,9-dimethyl-9,10-dihydroacridine (327 mg, 1.57 mmol, 2 eq.) were dried under vacuum for 30 min in a two-neck 100 mL round-bottomed flask fitted with a reflux condenser. The flask was back-filled with argon and dry toluene (20 mL) was added *via* syringe. The reaction mixture was bubbled with argon for 30 min, then $Pd_2(dba)_3{\cdot}CHCl_3$ (41 mg, 39 μmol, 0.05 eq.) and HP^{t}Bu$_3$BF$_4$ (23 mg, 79 μmol, 0.10 eq.) were added and the reaction mixture was bubbled with argon for a further 30 min. NaO^{t}Bu (225 mg, 2.34 mmol, 3 eq.) was added under a high flow of argon and the reaction was then heated to 115 °C (DrySyn kit temperature) with stirring for 17 h. At

the end of the reaction CH_2Cl_2 (70 mL) was added followed by water (70 mL). The organic layer was separated and the aqueous layer was extracted further with CH_2Cl_2 (2 × 70 mL). The organic extracts were combined, and were dried with $MgSO_4$ and filtered. The solvent was removed under reduced pressure and the crude mixture was purified by silica gel column chromatography with gradient elution from 20% CH_2Cl_2/hexane switching to 25% CH_2Cl_2. Removal of solvent under reduced pressure gave a yellow solid. Recrystallization by addition of hexane to a concentrated solution of product in CH_2Cl_2 gave **DAc-DBT** as a white crystalline solid (205 mg, 45%). Crystals suitable for X-ray diffraction were obtained by slow evaporation from CD_2Cl_2 and allowing for solvent evaporation. ^{1}H NMR (600 MHz, CD_2Cl_2) δ 8.20 (d, 2H, *J* = 8.4 Hz), 8.11 (d, 2H, *J* = 1.9 Hz), 7.48 (dd, 2H, *J* = 8.4, 1.9 Hz), 7.47 – 7.43 (m, 4H), 6.96 – 6.85 (m, 8H), 6.33 – 6.26 (m, 4H), 1.67 (s, 12H); ^{13}C NMR (151 MHz, CD_2Cl_2) δ 141.5, 140.2, 138.7, 138.1, 130.8, 130.6, 126.7, 125.8, 125.6, 125.3, 121.0, 114.5, 36.3, 31.3; HRMS-ASAP-TOF$^+$ *m/z* calculated for $C_{42}H_{34}N_2S$ $[M]^+$ 598.2437, found: 598.2428 ; Anal. Calc. for $C_{42}H_{34}N_2S$ C, 84.24; H, 5.72; N. 4.68. Found: C, 84.14; H, 5.61; N, 4.56; m.p. 333.4 – 335.0 °C.

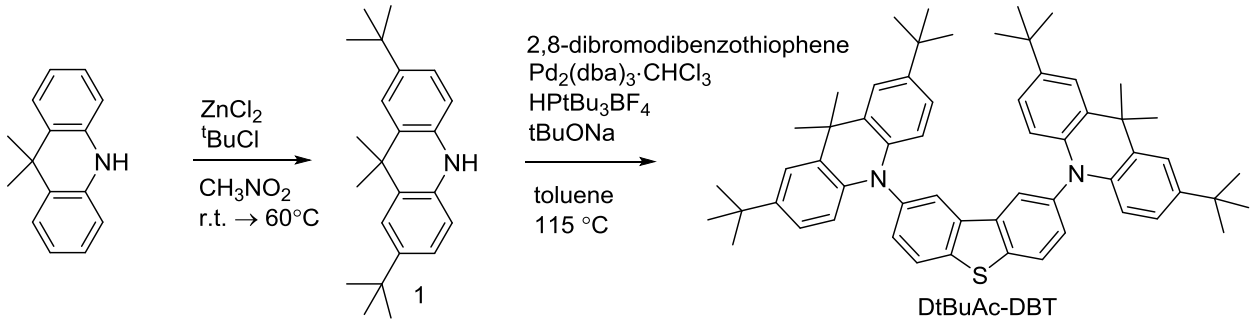

2,7-Di-(tert-butyl)-9,9-dimethylacridine (1)

To a stirring solution of 9,10-dihydro-9,9-dimethylacridine (0.50 g, 2.38 mmol) and $ZnCl_2$ (0.32 g, 2.38 mmol)) in nitromethane (50 mL), ^{t}BuCl (0.55 mL, 5.06 mmol) in a two-neck round-bottom flask was added dropwise under argon atmosphere. After being stirred at 60 °C for 20 h, the reaction mixture was extracted with dichloromethane (3 × 80 mL) and neutralized with the aqueous solution of $NaHCO_3$ (100 mL). Precipitation of the crude product on crushed ice, followed by filtration and drying under vacuum, yielded the product (0.75 g, 98%). ^{1}H NMR (400 MHz, acetone-d_6) δ: 7.45 (d, 2H, *J* = 2.2 Hz), 7.10 (dd, 2H, *J* = 8.3 Hz, *J* = 2.2 Hz), 6.74 (dd, 2H, *J* = 8.3 Hz, *J* = 1.0 Hz), 1.59 (s. 6H), 1.31 (s, 18H). ^{13}C{^{1}H} NMR (400 MHz, acetone-d_6) δ: 141.9, 123.3, 121.9, 112.8, 36.3, 33.9, 31.1. HRMS-ASAP m/z calculated for $C_{23}H_{31}N$ [M]+ 321.2457, found: 321.2441.

2,8-Bis(2,7-di(tert-butyl)-9,9-dimethylacridin-10(9H)-yl)dibenzo[b,d]thiophene (DtBuAc-DBT)

2,8-Dibromodibenzothiophene (0.17 g, 0.77 mmol, 1 eq.) and compound **1** (0.50 g, 1.55 mmol, 2.2 eq.) were dried under vacuum for 30 min in a two-neck round-bottomed 100 mL flask fitted with a reflux condenser. The flask was back-filled with argon for 30 min, then $Pd_2(dba)_3$·$CHCl_3$ (0.04 g, 0.038 mmol, 0.05 eq.) and HP^{t}Bu$_3$BF$_4$ (22 mg, 0.07 mmol, 0.1 eq.)

were added and the reaction mixture was bubbled with argon for 30 min. ^{t}BuONa (0.22 g, 2.33 mmol, 3 eq.) was added under a high flow of argon and the reaction was heated then to 115°C (DrySyn kit temperature) with stirring for 17 h. After being cooled to room temperature, the reaction mixture was extracted with CH_2Cl_2 (3 × 100 mL). The organic layer was dried with $MgSO_4$ and filtered. The solvent was removed under reduced pressure and the crude mixture was purified by silica gel chromatography with gradient elution from 40% *v/v* CH_2Cl_2/hexane switching to 100% CH_2Cl_2 in 20% increasing increments. Removal of solvent under reduced pressure resulted in product as a white solid. Recrystallization from boiling hexane with dropwise addition of CH_2Cl_2 followed by cooling to 0 °C gave pure product as a white crystalline solid (0.32 g, 51%). Crystals suitable for X-ray diffraction were obtained by slow evaporation from CH_2Cl_2 / hexane mixture of solvents. ^{1}H NMR (400 Hz, CD_2Cl_2) δ: 8.22 (d, 2H, *J* = 8.4 Hz), 8.09 (d, 2H, *J* = 2.0 Hz), 7.47-7.51 (m, 6H), 6.97 (dd, 4H, *J* = 8.7 Hz, *J* = 2.3 Hz), 6.24 Hz (d, 4H, *J* = 9.0 Hz), 1.72 (s, 12 H), 1.30 (s, 36H). ^{13}C{^{1}H} NMR (400 Hz, CD_2Cl_2) δ: 143.4, 140.0, 139.1, 138.1, 130.8, 129.9, 129.4, 125.6, 125.3, 123.5, 122.6, 113.9, 36.8, 34.5, 31.8, 31.6. HRMS-ASAP-TOF^{+} m/z calculated for $C_{56}H_{32}N_6$ [M]+ 823.4980, found: 823.5018. Anal. Calc. for $C_{56}H_{32}N_6$: C, 84.62; H, 8.08; N, 3.40. Found: C, 84.48; H, 8.02; N, 3.27. m.p. = 255-257 °C.

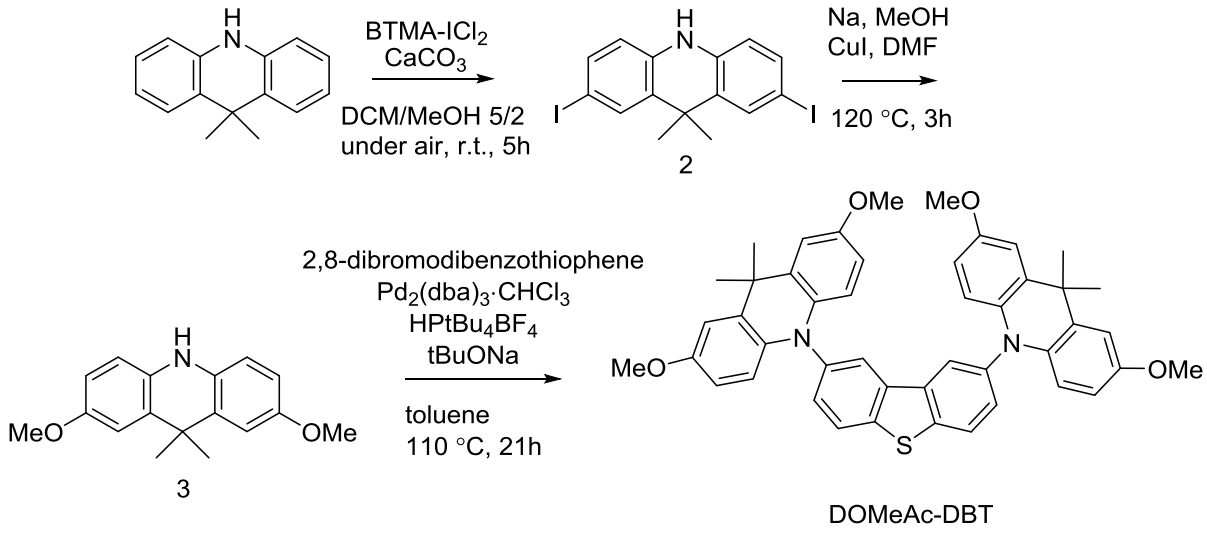

9,9-Dimethyl-9,10-dihydroacridine was prepared according to the literature procedure.[2]

2,7-Diiodo-9,9-dimethyl-9,10-dihydroacridine (2)

Compound **2** was prepared according to the literature procedure[3]. To a solution of 9,9-dimethyl-9,10-dihydroacridine (1.00 g, 5.62 mmol) in dichloromethane (100 mL) and methanol (40 mL) mixture was added BTMA-ICl_2 (4.10 g, 11.80 mmol) and calcium carbonate (1.18 g, 11.8 mmol). The mixture was stirred for 5 h at room temperature. Excess calcium carbonate was filtered off and the filtrate was concentrated under reduced pressure. Afterwards, the residue was neutralized with the aqueous $NaHSO_3$ solution and extracted with diethyl ether (3 × 100 mL). The ether layer was dried with $MgSO_4$ and evaporated in vacuum to give the target compound as colourless powder (1.62 g, 63%). ^{1}H NMR (400

MHz, acetone-d_6) δ: 8.41 (s, 1H), 7.69 (d, 2H, *J* = 2.0 Hz), 7.40 (dd, 2H, *J* = 8.3 Hz, *J* = 2.0 Hz), 6.69 (d, 2H, *J* = 8.4 Hz), 1.57 (s, 6H). $^{13}C\{^1H\}$ NMR (400 Hz, acetone-d_6) δ: 138.4, 135.6, 134.1, 131.2, 116.1, 81.3, 35.9, 30.2. HRMS-ASAP+ m/z calculated for $C_{15}H_{13}I_2N$ [M]+ 461.9171, found: 461.9216.

2,7-Dimethoxy-9,9-dimethyl-9,10-dihydroacridine (3)

DMF (15 mL), CuI (1.65 g, 8.66 mmol) and compound **2** (1.00 g, 2.16 mmol) were added to a solution of metallic sodium (0.99 g, 43.2 mmol) in dry methanol (6 mL). The reaction mixture was refluxed for 3 h under argon atmosphere. After the reaction, EtOAc was added to the reaction mixture and the insoluble materials were filtered through Celite™ and washed through with EtOAc (70 mL). The filtrate was washed with brine (100 mL), dried over $MgSO_4$, filtered and concentrated. The residue was purified by column chromatography using 10:1 hexane:EtOAc *(v/v)* as the eluent to give the product as yellow oil (0.41 g, 70.5%). ^1H NMR (400 Hz, acetone-d_6) δ: 7.65 (s, 1H), 6.98 (d, 2H, *J* = 2.7 Hz), 6.75 (dd, 2H, *J* = 8.7 Hz, *J* = 1.7 Hz), 6.69 (dd, 2H, *J* = 8.6 Hz, *J* = 2.7 Hz), 3.75 (s, 6H), 1.55 (s, 6H). $^{13}C\ \{^1H\}$ NMR (400 Hz, acetone-d_6) δ: 153.8, 133.9, 128.9, 113.8, 112.2, 111.1, 54.9, 36.6, 29.4. HRMS-ASAP+ m/z calculated for $C_{17}H_{19}NO_2$ [M]+ 270.1449, found: 270.1470.

2,8-Bis(2,7-dimethoxy-9,9-dimethylacridin-10(9H)-yl)dibenzo[b,d]thiophene (DOMeAc-DBT)

2,8-Dibromodibenzothiophene (0.23 g, 0.67 mmol, 1 eq.) and 2,7-dimethoxy-9,9-dimethyl-9,10-dihydroacridine (0.40 g, 1.48 mmol, 2.2 eq.) were dried under vacuum for 30 min in a two-neck round-bottomed 100 mL flask fitted with a reflux condenser. The flask was back-filled with argon for 30 min, then toluene (25 mL), $Pd_2(dba)_3{\cdot}CHCl_3$ (35 mg, 0.03 mmol, 0.05 eq.) and $HP^tBu_3BF_4$ (19 mg, 0.067 mmol, 0.1 eq.) were added and the reaction mixture was bubbled with argon for 30 min. *t*BuONa (0.194 g, 2.02 mmol, 3 eq.) was added under a high flow of argon and the reaction was heated then to 115 ^oC (DrySyn kit temperature) with stirring for 21 h. After being cooled to room temperature, the reaction mixture was extracted with EtOAc (3 × 100 mL). The organic layer was dried above $MgSO_4$ and filtered. The solvent was removed under reduced pressure and the crude mixture was purified by silica gel chromatography with gradient elution from 60% *v/v* CH_2Cl_2/hexane switching to 100% CH_2Cl_2 in 20% increasing increments. Removal of solvent under reduced pressure resulted in a crude product as a light yellow solid. A solution of the obtained solid in CH_2Cl_2 was added into methanol to precipitate the product as a light yellow solid (0.32 g, 66%). ^1H NMR (400 Hz, CD_2Cl_2) δ: 8.20 (d, 2H, *J* = 8.4 Hz), 8.12 (d, 2H, *J* = 1.9 Hz), 7.59 (dd, 2H, *J* = 8.4 Hz, *J* = 2.0 Hz), 7.05 (d, 4H, *J* = 2.8 Hz), 6.54 (dd, 4H, *J* = 8.9 Hz), 6.28 (d, 4H, *J* = 8.9 Hz), 3.74 (s, 12H), 1.69 (s, 12H). $^{13}C\ \{^1H\}$ NMR (400 Hz, CD_2Cl_2) δ: 154.0, 139.4, 139.0, 137.5, 135.9, 131.0, 130.3, 124.99, 124.8, 114.6, 111.4, 111.1, 55.5, 36.5, 30.1. HRMS-ASAP-TOF$^+$ m/z calculated for $C_{46}H_{42}N_2O_4S$ $[M]^+$ 719.2899, found:719.2902. Anal. Calc. for $C_{46}H_{42}N_2O_4S$: C, 76.85; H, 5.89; N, 3.73. Found: C, 76.46; H, 5.63; N, 3.73. m.p. = 249–251 ^oC.

S1c. ^{1}H and ^{13}C NMR spectra of the synthesized compounds

2,8-Bis(9,9-dimethylacridin-10(9H)-yl)dibenzo[b,d]thiophene (DAc-DBT)

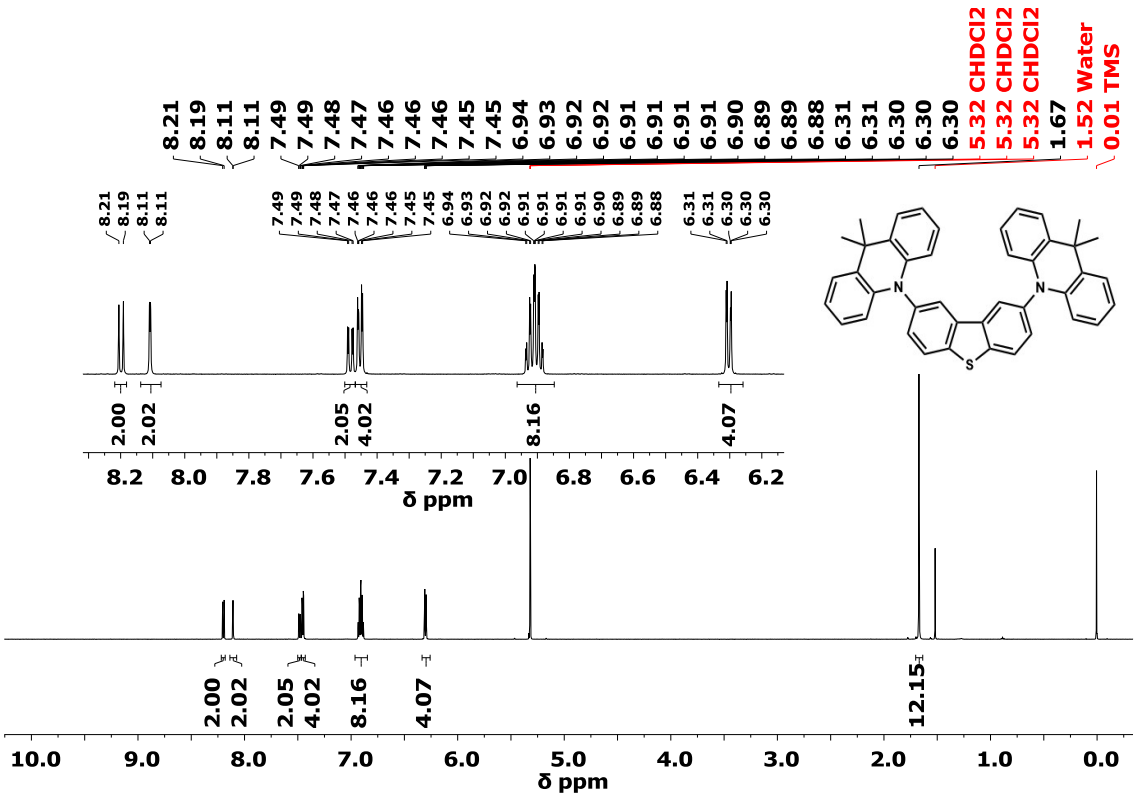

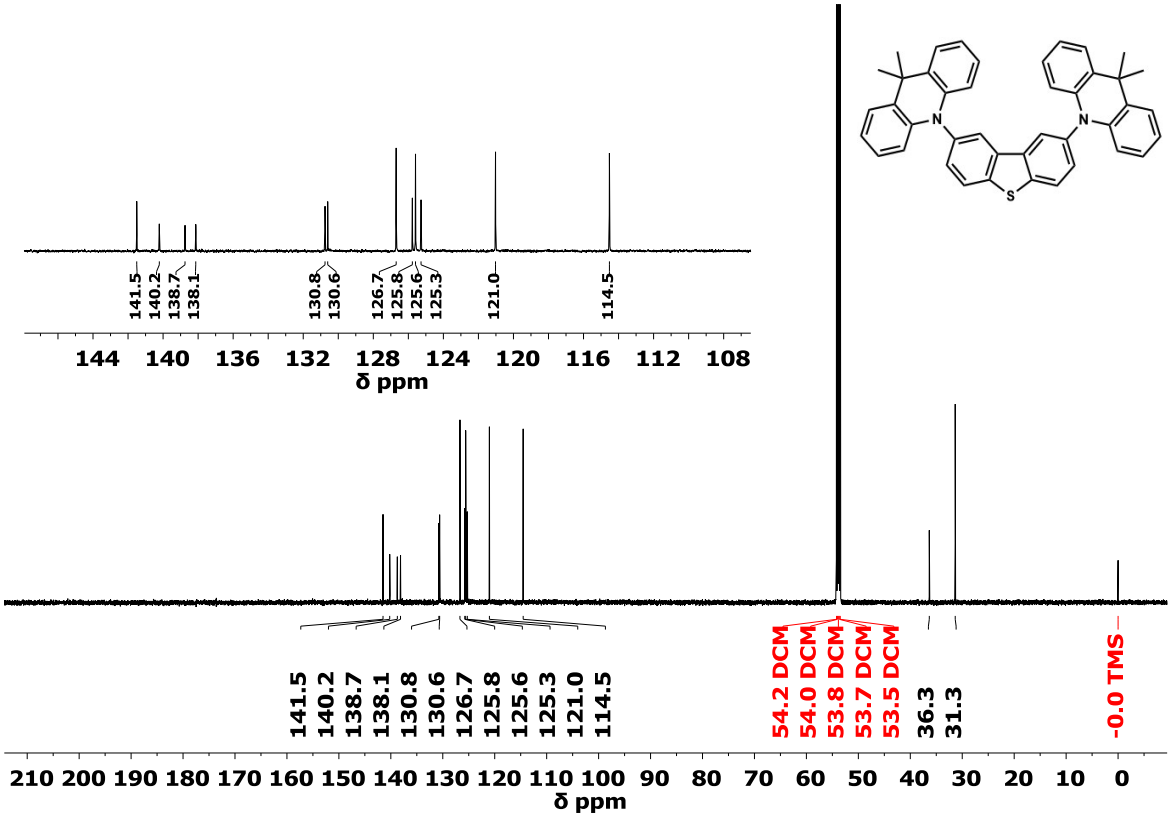

2,7-Di-(tert-butyl)-9,9-dimethylacridine (1)

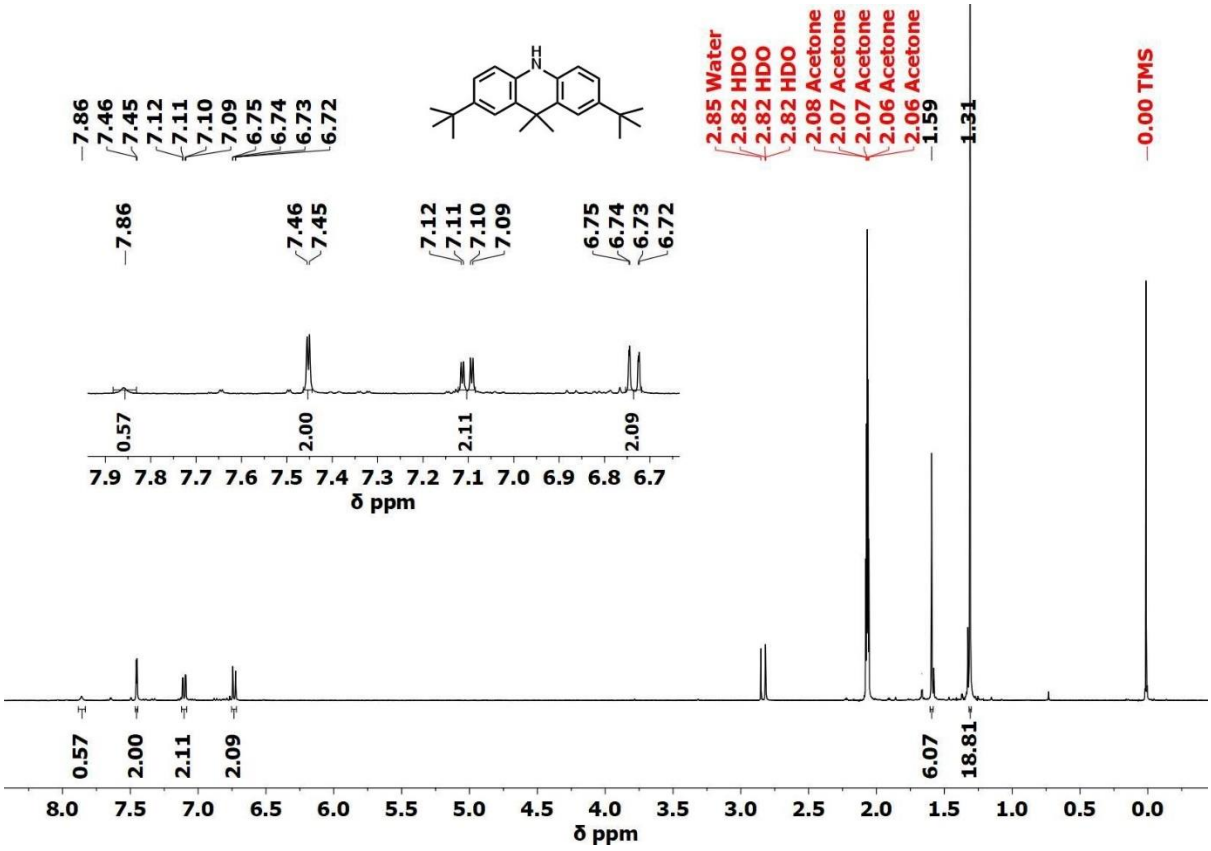

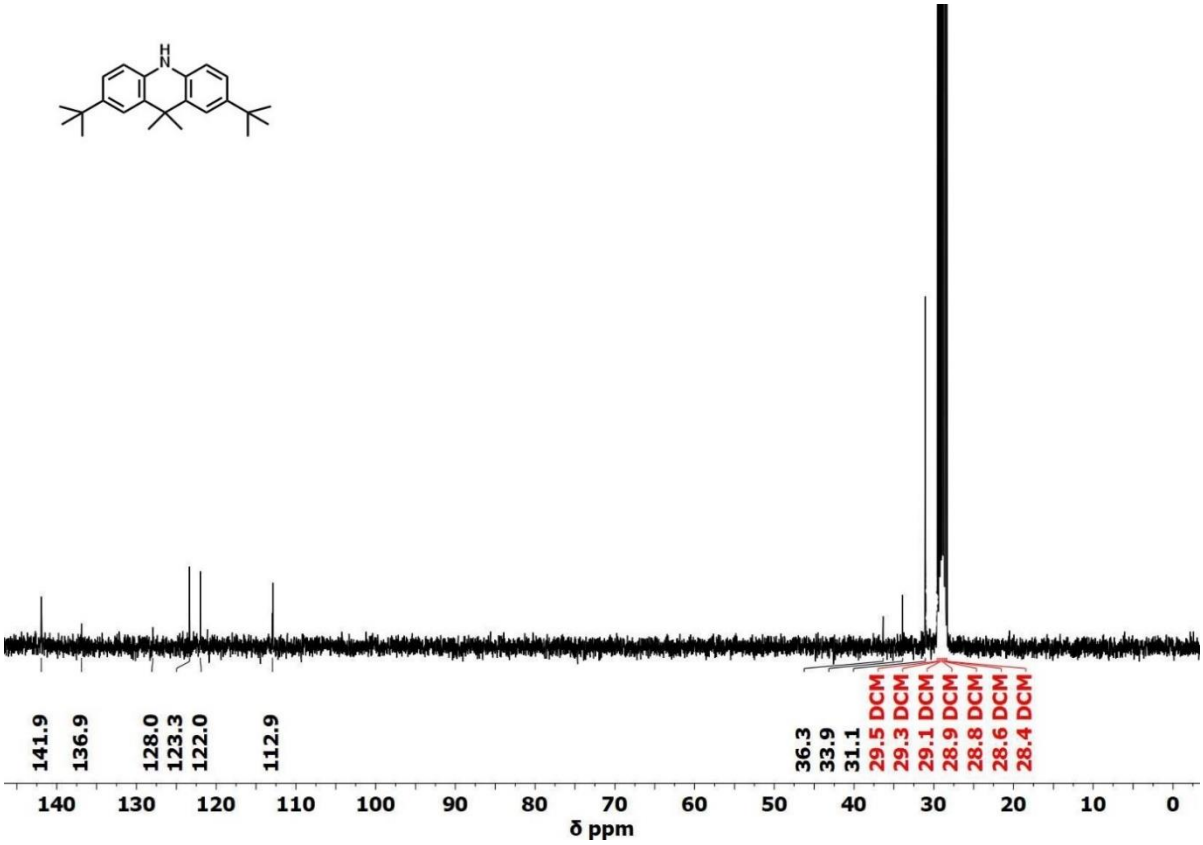

2,8-Bis(2,7-di(tert-butyl)-9,9-dimethylacridin-10(9H)-yl)dibenzo[b,d]thiophene (DtBuAc-DBT)

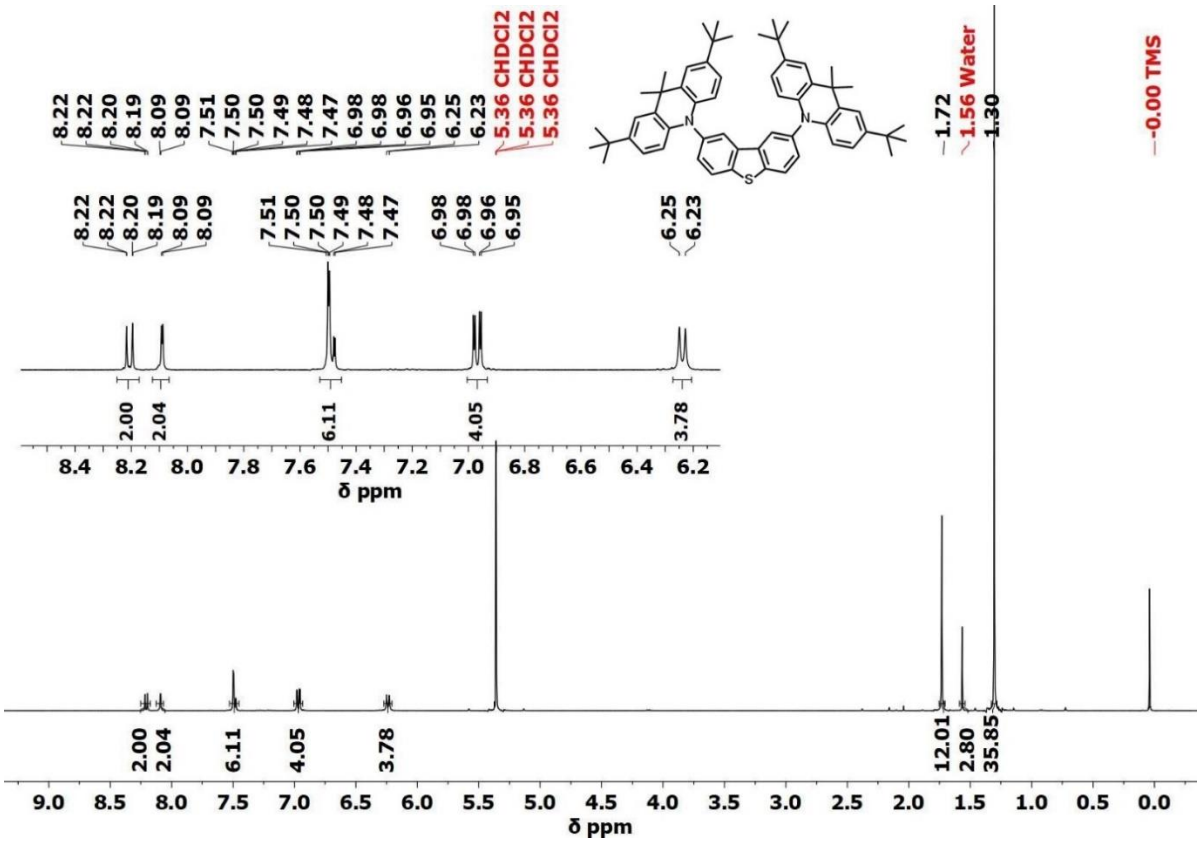

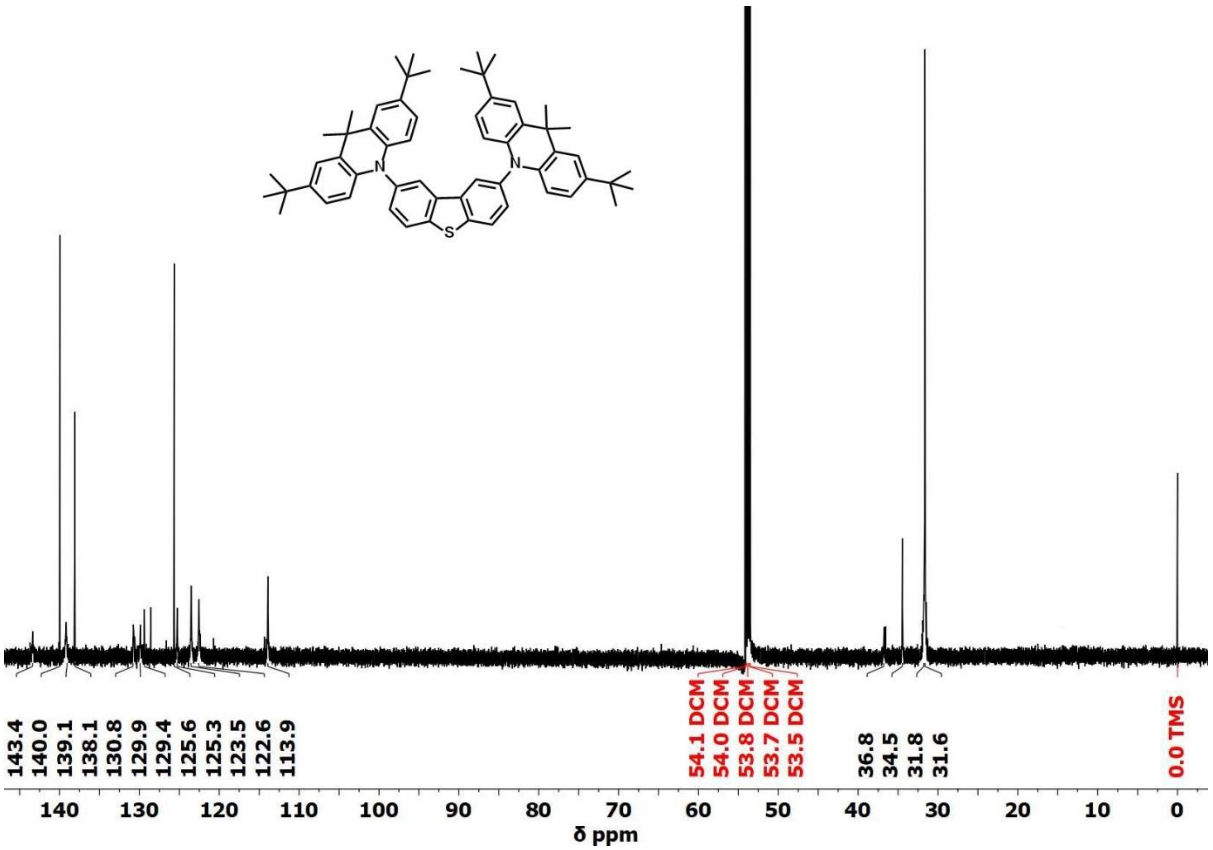

2,7-Diiodo-9,9-dimethyl-9,10-dihydroacridine (2)

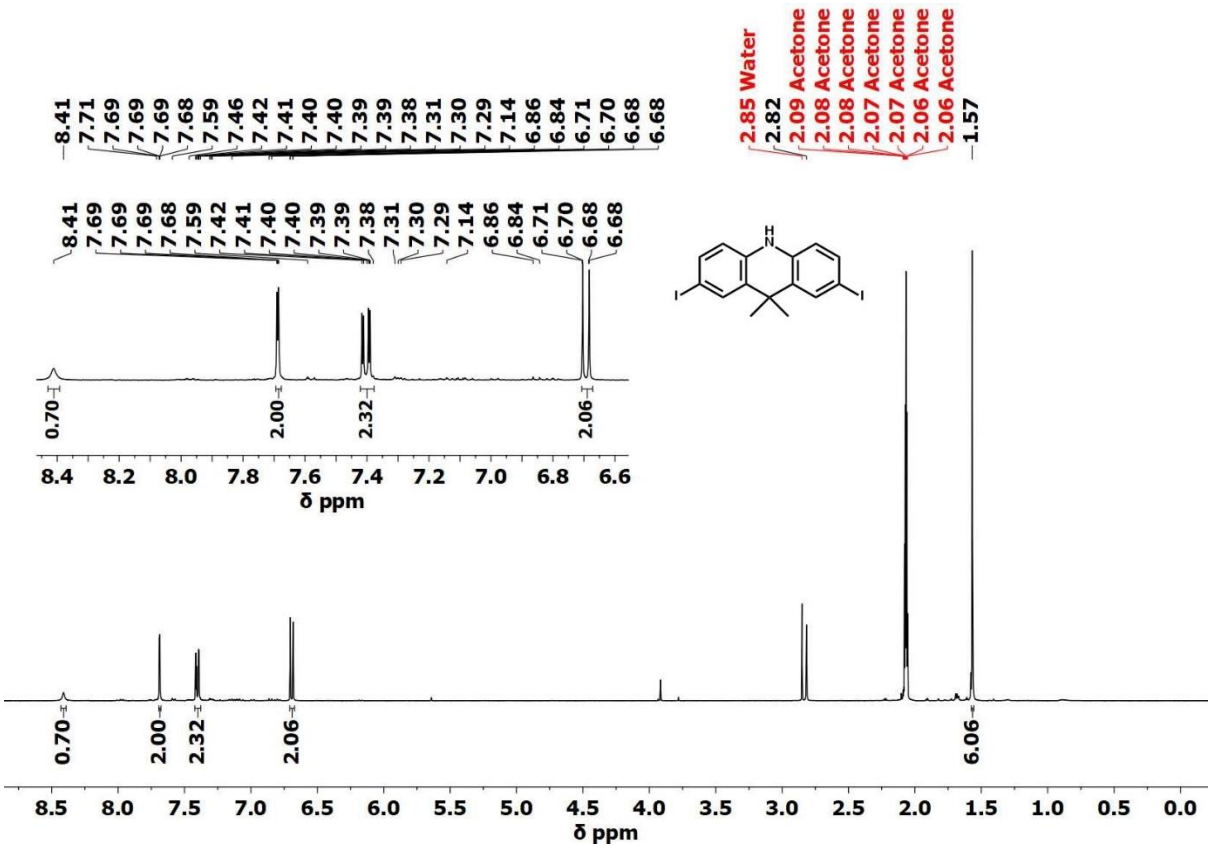

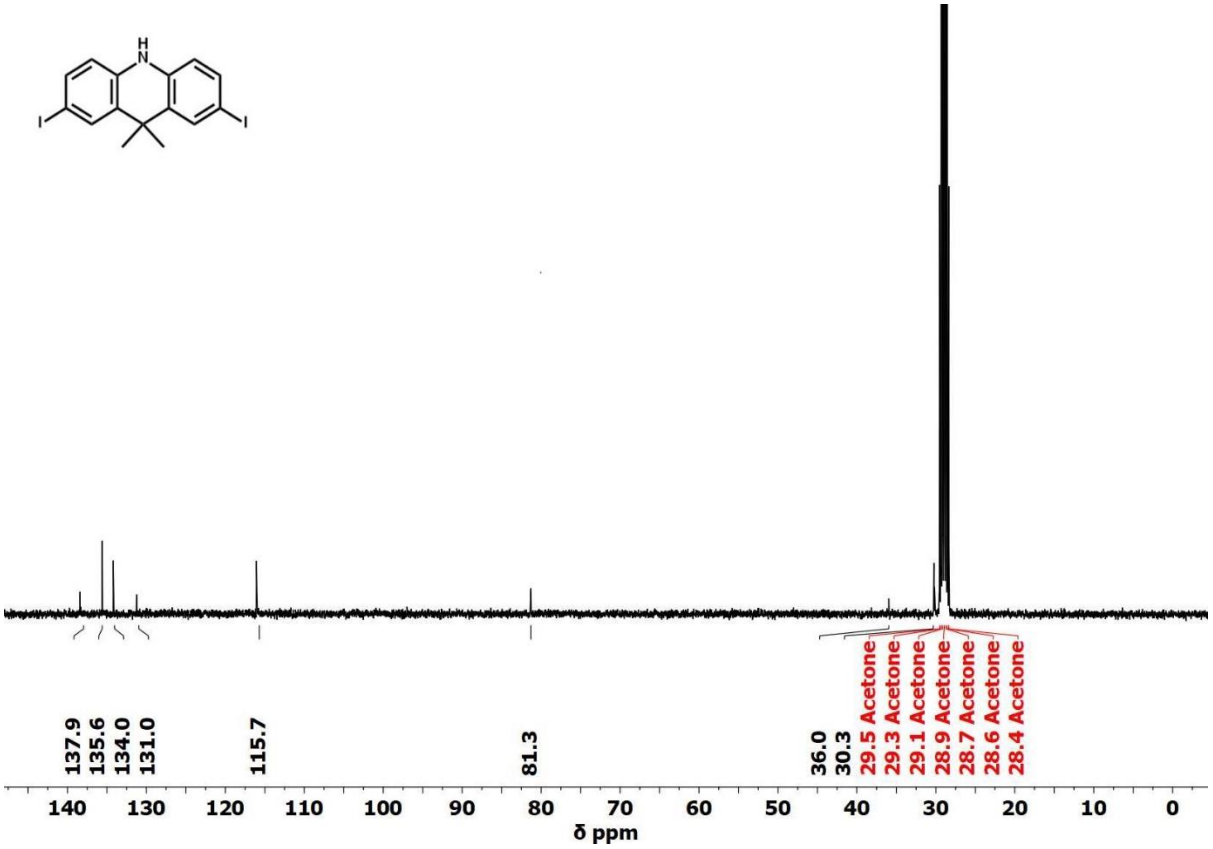

2,7-Dimethoxy-9,9-dimethyl-9,10-dihydroacridine (3)

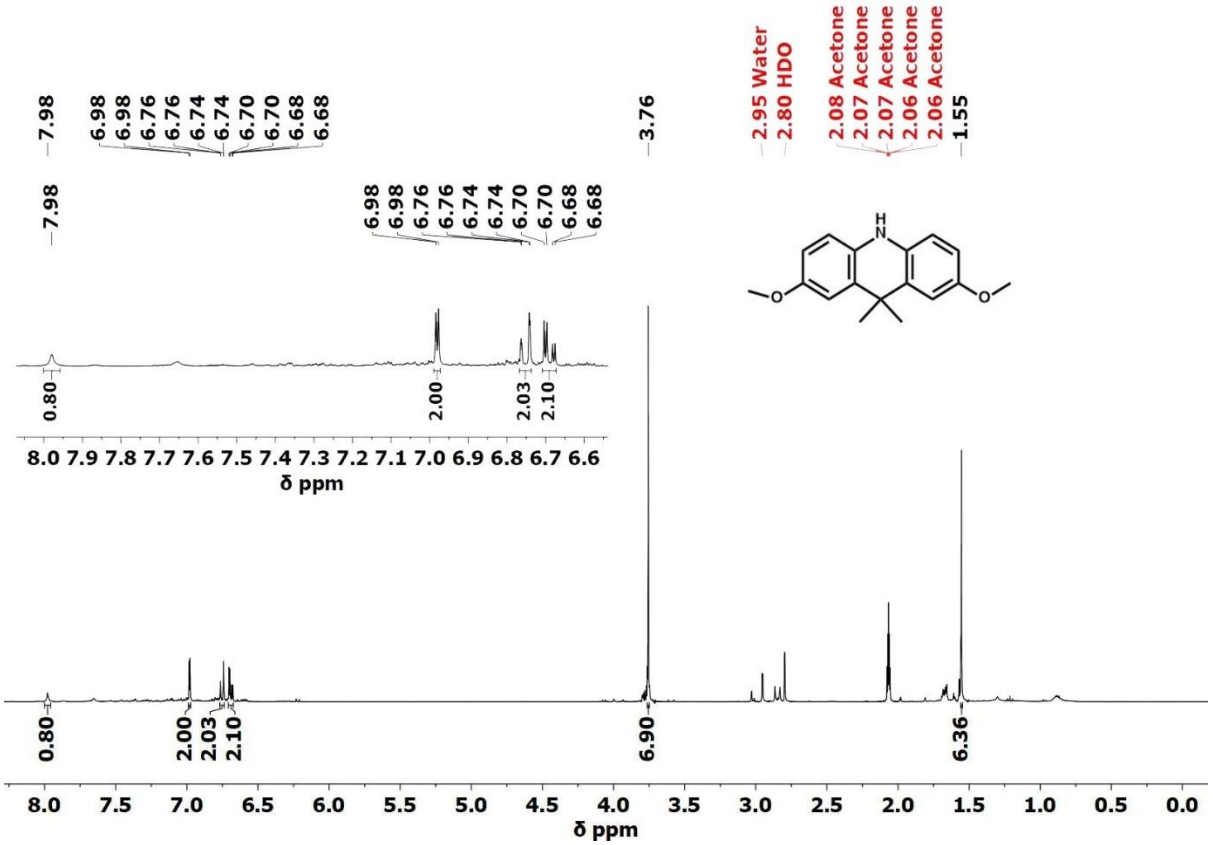

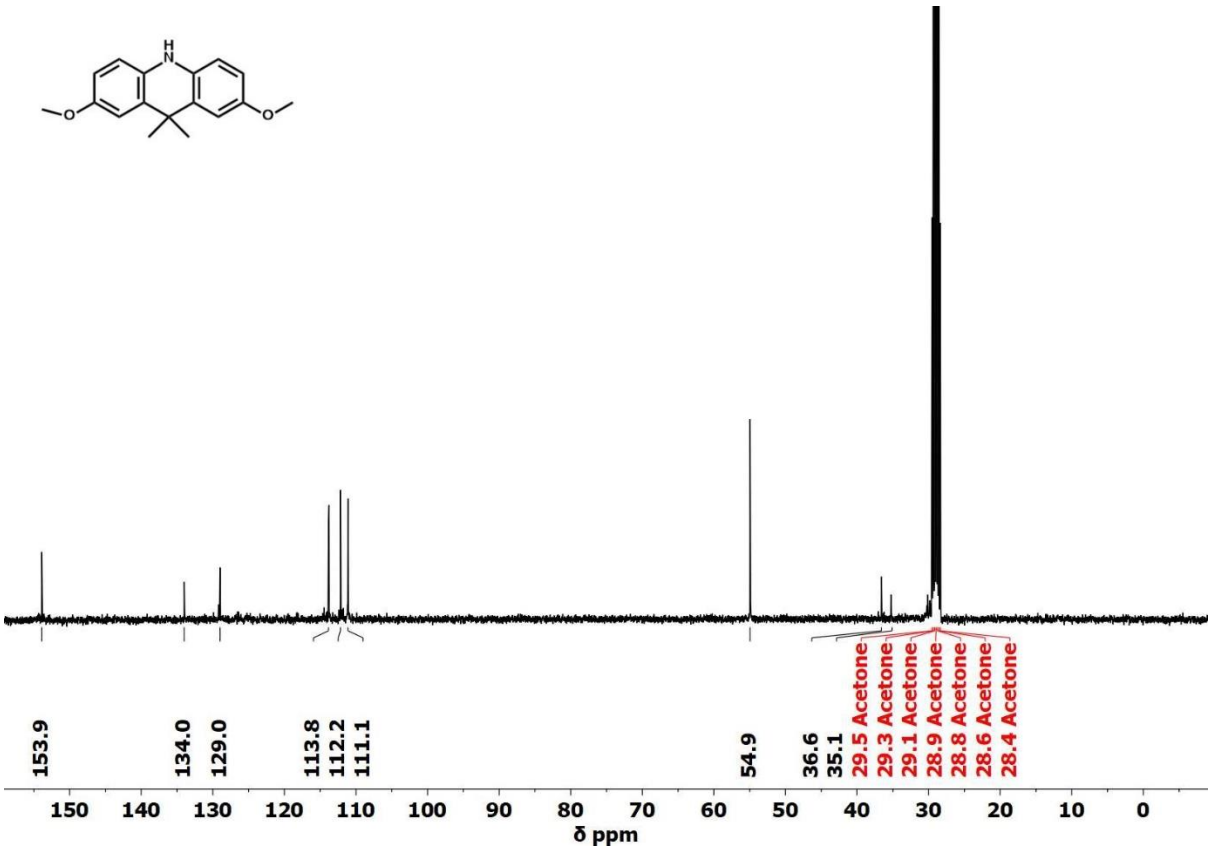

2,8-Bis(2,7-dimethoxy-9,9-dimethylacridin-10(9H)-yl)dibenzo[b,d]thiophene (DOMeAc-DBT)

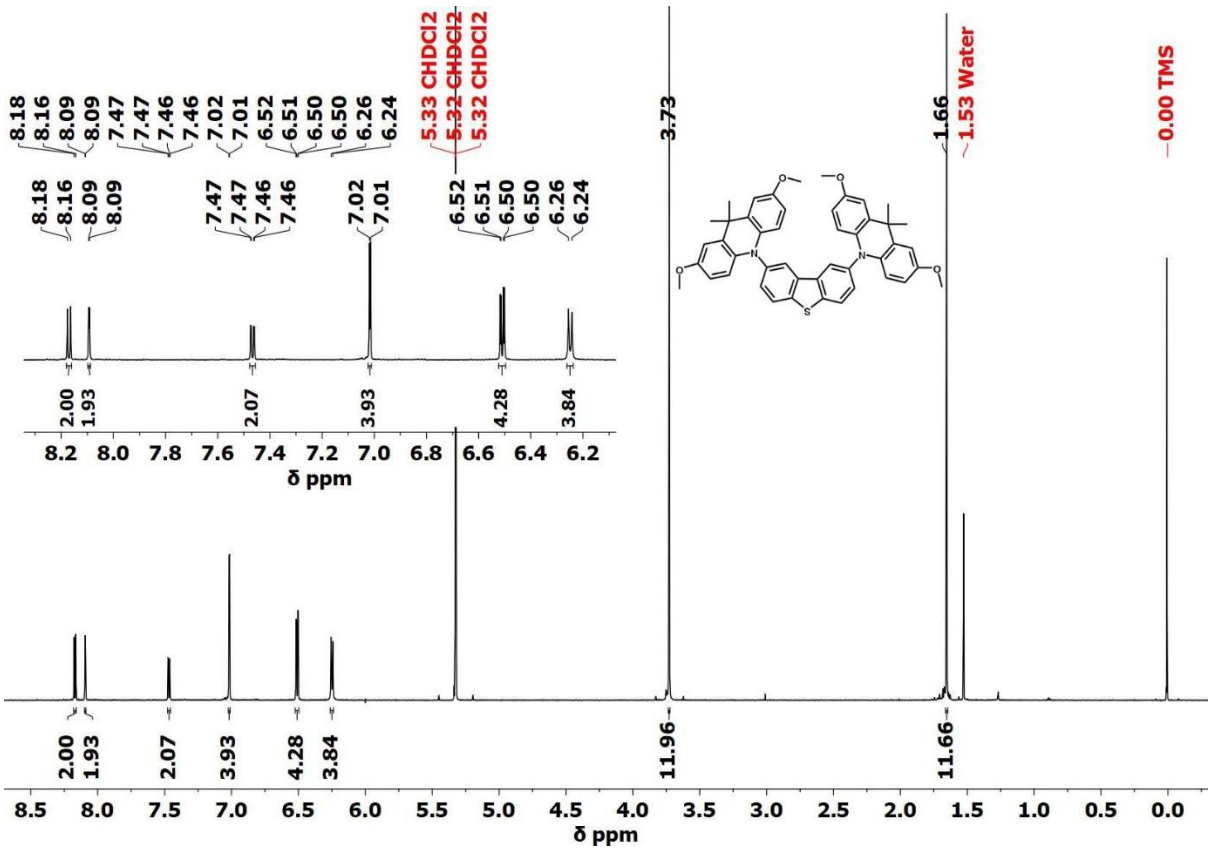

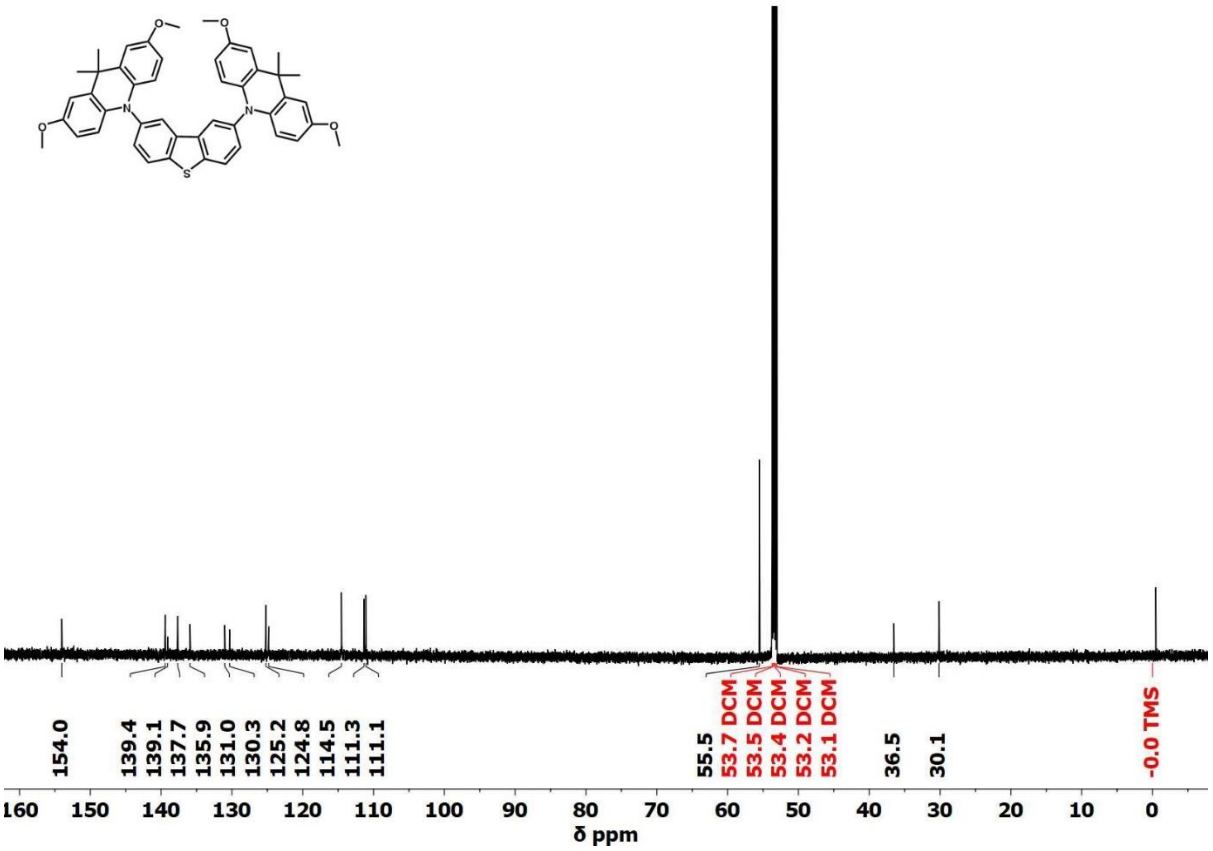

S2. X-Ray Crystallography

X-ray single crystal data were collected on a Bruker 3-circle D8 Venture diffractometer with a Photon100 CMOS detector, using Mo-$K\alpha$ radiation (λ = 0.71073 Å) from a IμS-microsource with focusing mirrors. The crystals were cooled with a Cryostream (Oxford Cryosystems) open-flow N_2 cryostat. The structures were solved by direct methods using SHELXS program, [4] and refined using SHELXL software[5] on OLEX2 platform.[6] Selected crystal data and experimental details are listed in Table S1, full crystallographic information (including structure factors) in CIF format has been deposited with Cambridge Crystallographic Data Centre.

DAc-DBT undergoes a reversible phase transition on cooling below 170 K, whereupon the structure is modulated with doubling of the *a* parameter. The room-temperature phase was characterized at 200 K and the low-temperature one at 120 K. The structure of **DtBuAc-DBT** was also determined at 120 and 200 K, but was found to be essentially the same at both temperatures.

Table S1. Crystal data and experimental details

Compound	**DAc-DBT**		**DtBAc-DBT**	
Formula	$C_{42}H_{34}N_2S{\cdot}CD_2Cl_2$		$C_{58}H_{66}N_2S$	
Molecular weight	685.71		823.18	
CCDC	1901568	1901569	1901570	1901571
$D_{calc.}$/ g cm^{-3}	1.304	1.289	1.124	1.143
μ/mm^{-1}	0.280	0.277	0.105	0.107
T/K	120	200	200	120
Crystal System	monoclinic	monoclinic	triclinic	triclinic
Space Group	$P2_1/n$ (no. 14)	$P2_1/n$ (no. 14)	P-1 (no. 2)	P-1 (no. 2)
a/Å	24.0937(12)	12.1029(6)	9.8347(4)	9.7054(5)
b/Å	7.9916(4)	8.0200(4)	12.1070(5)	12.0521(6)
c/Å	36.7515(18)	36.8781(19)	21.2839(9)	21.3945(10)
α/°	90	90	83.6588(19)	83.6147(19)
β/°	99.3094(16)	99.1232(15)	88.476(2)	88.817(2)
γ/°	90	90	74.8909(19)	74.1306(18)
V/Å^3	6983.2(6)	3534.3(3)	2431.67(18)	2392.1(2)
Z	8	4	2	2
Θ_{max}/°	25.7	25	25	25
Measured Refl.	88992	34143	27673	37697
Independent Refl.	13247	6222	8540	8436
with $I > 2(I)$	9504	4363	5863	6465
R_{int}	0.064	0.052	0.038	0.038
Parameters/restraints	903, 18	465, 17	628, 38	631, 38
$\Delta\rho_{max,min}$ /eÅ^{-3}	0.34, -0.51	0.25, -0.29	0.28, -0.21	0.34, -0.25
Goodness of fit	1.013	1.042	1.030	1.027
R_1, wR_2 (all data)	0.077, 0.114	0.083, 0.116	0.084, 0.137	0.065, 0.115
R_1, wR_2 [$I > 2(I)$]	0.047, 0.102	0.050, 0.103	0.051, 0.123	0.044, 0.105

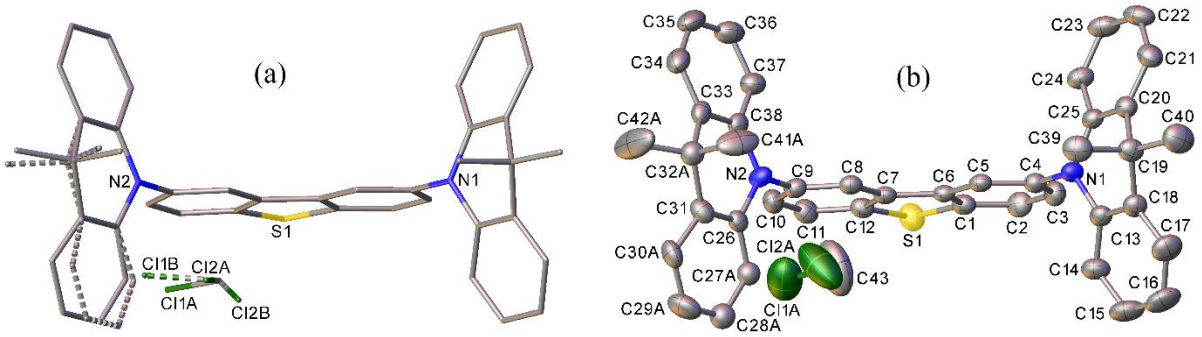

Figure S1. X-ray molecular structure of **DAc-BDT**·CD_2Cl_2 at 200 K;. (a): disorder, (b): major conformation only. Thermal ellipsoids are drawn at the 50% probability level, H atoms are omitted for clarity.

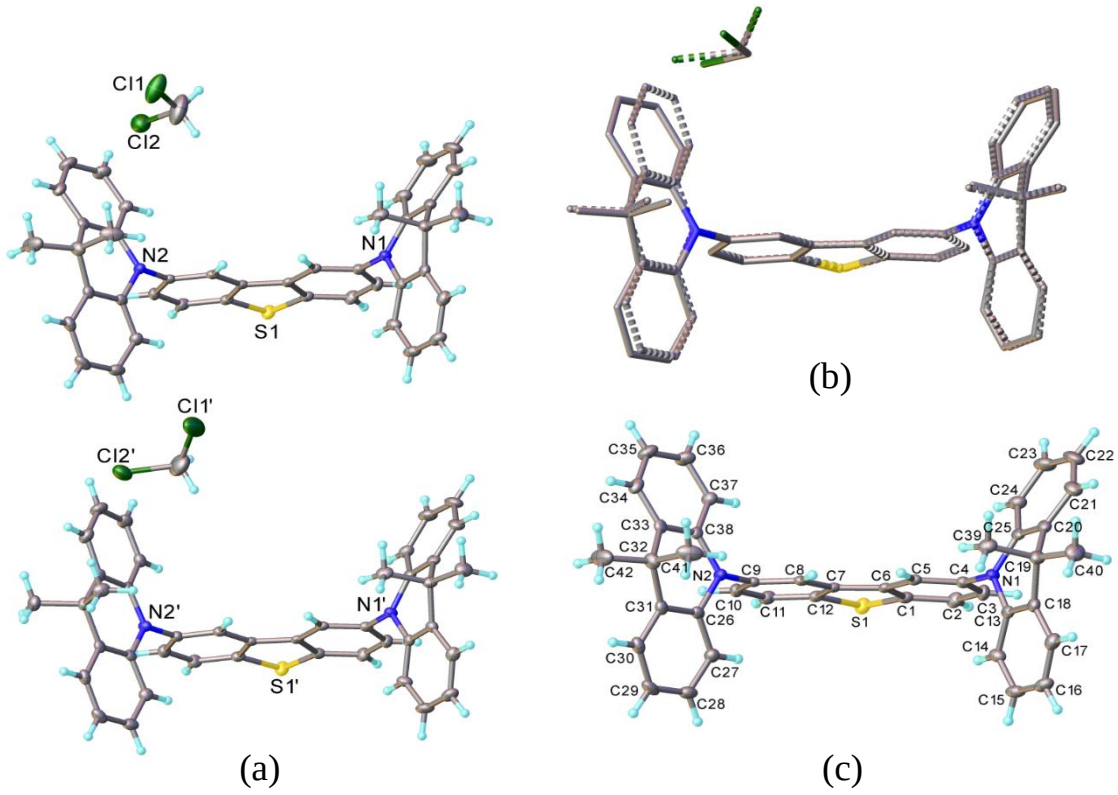

Figure S2. (a) The asymmetric unit in the crystal of **DAc-BDT**·CD_2Cl_2 at 120 K, (b) the same overlaid by a shift of *a*/2 (H atoms are omitted), (c) atom numbering in one independent molecule. Thermal ellipsoids are drawn at the 50% probability level.

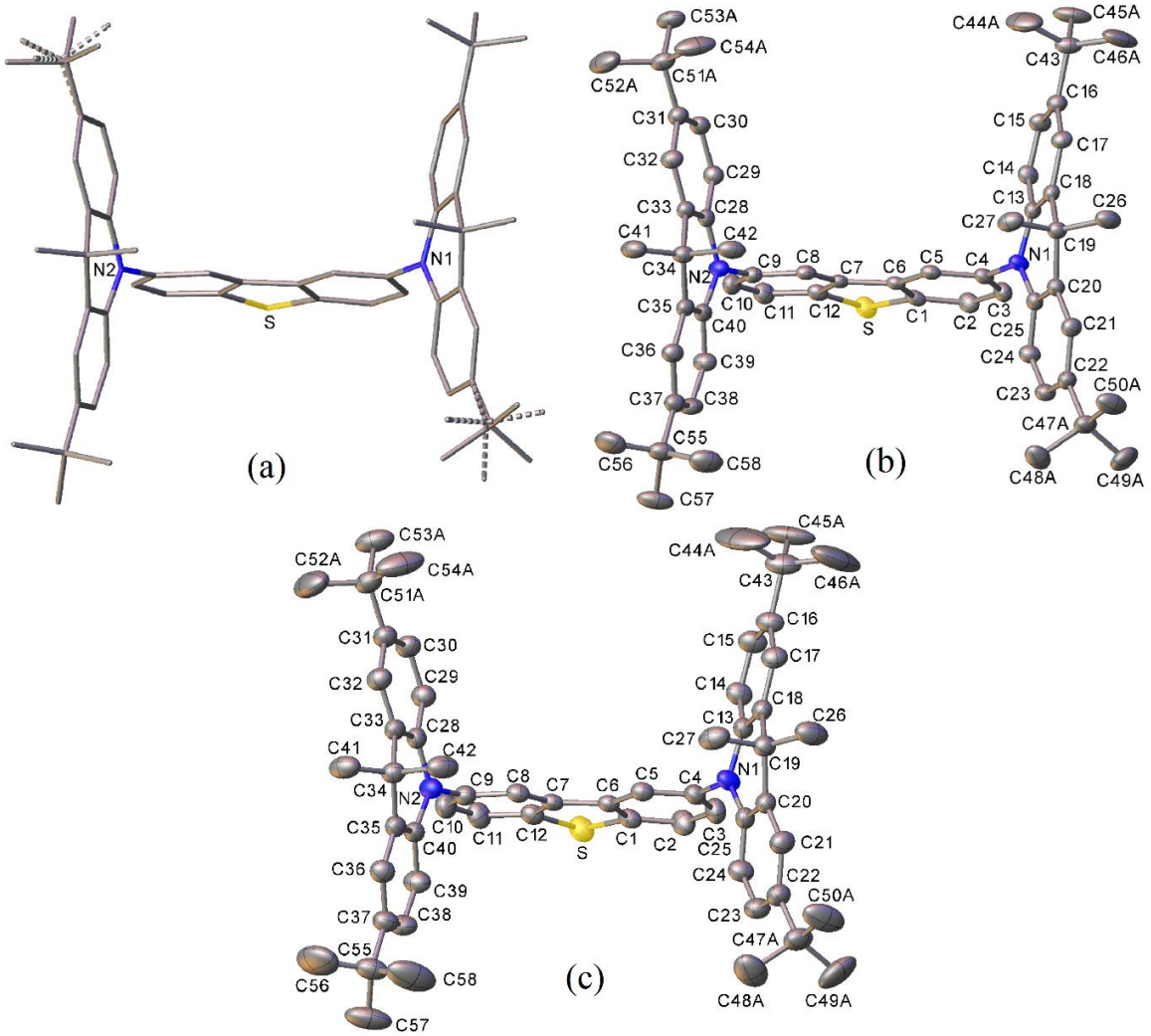

Figure S3. X-ray molecular structure of **DtBuAc-BDT**: (a) disorder, (b) major conformation at 120 K (c) the same at 200 K. Thermal ellipsoids are drawn at the 50% probability level, H atoms are omitted for clarity.

S3. Computational Details

Computations were performed with the Gaussian 09 package[7] using various density functional theory (DFT) methods. The isolated molecules were optimized at the rBMK/6-31G(d) level in gas phase. The spectroscopic properties of the molecules were calculated by means of time-dependent DFT (TD-DFT)[8] calculations employing 6-31G(d) basis set. The BMK functional was preferred for the geometry optimization and the prediction of the optical properties of all the studied molecules as it was shown to be pertinent for the description of the low energy band in the absorption of D–A CT compounds.[9–11] Multiwfn[12] software was used to evaluate molecular fragment contributions to occupied and virtual orbitals.

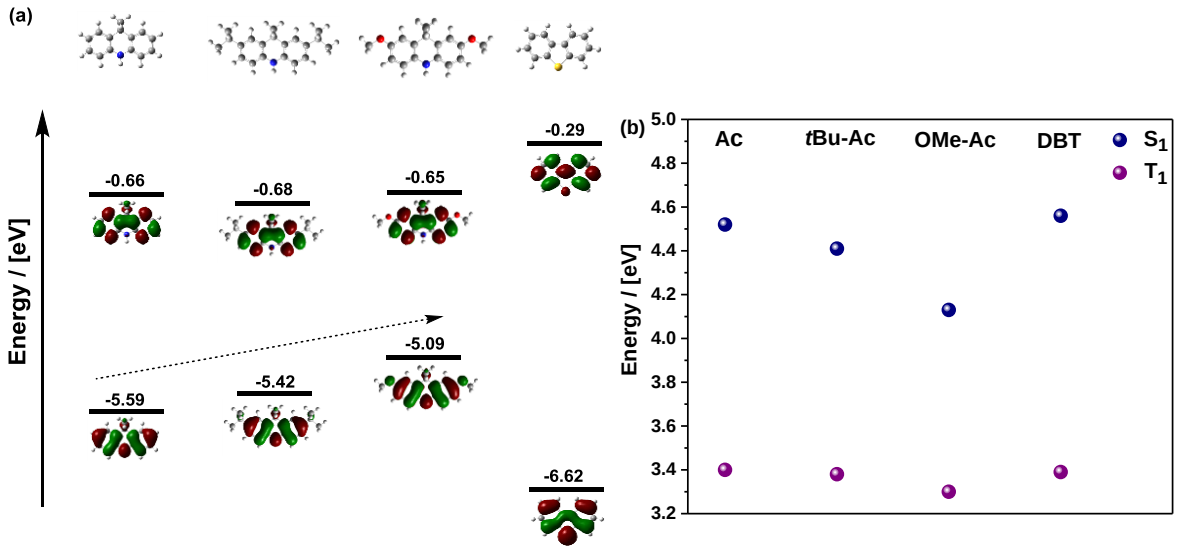

Figure S4. (a) Optimized structures along with HOMO/LUMO profiles and energies and (b) singlet and triplet energy diagram of Ac, tBu-Ac, OMe-Ac and DBT fragments (rBMK/6-31G (d)).

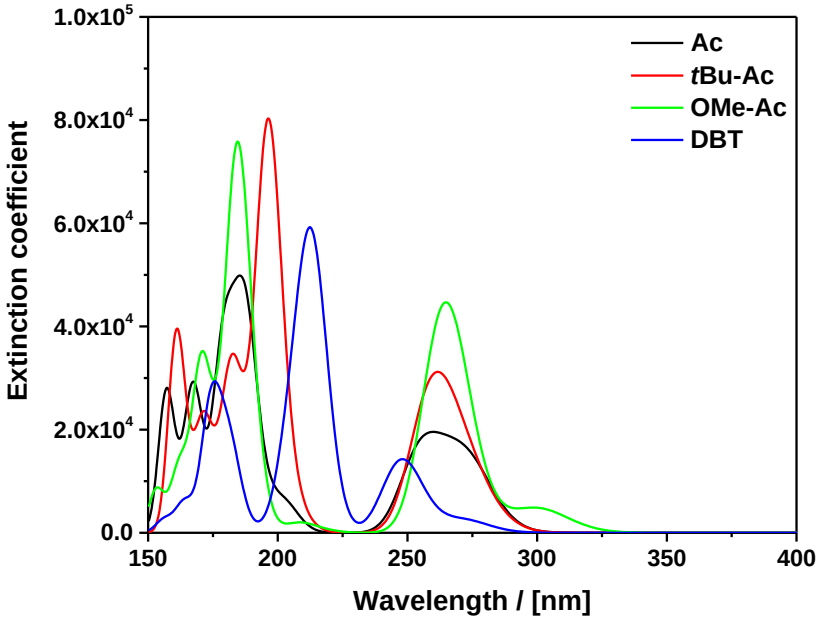

Figure S5. Theoretically predicted absorption spectra of Ac, tBu-Ac, OMe-Ac and DBT units (TD-DFT rBMK/6-31G (d)).

Table S2. Donor and acceptor contributions to the HOMO and LUMO of **DAc-DBT**, **DtBuAc-DBT** and **DOMeAc-DBT.**

Molecule/moiety	DBT		Donors	
	HOMO / [%]	LUMO / [%]	HOMO / [%]	LUMO / [%]
DAc-DBT	4.794	94.687	95.204	5.347
DtBuAc-DBT	4.572	94.878	95.411	5.154
DOMeAc-DBT	4.160	94.691	95.832	5.343

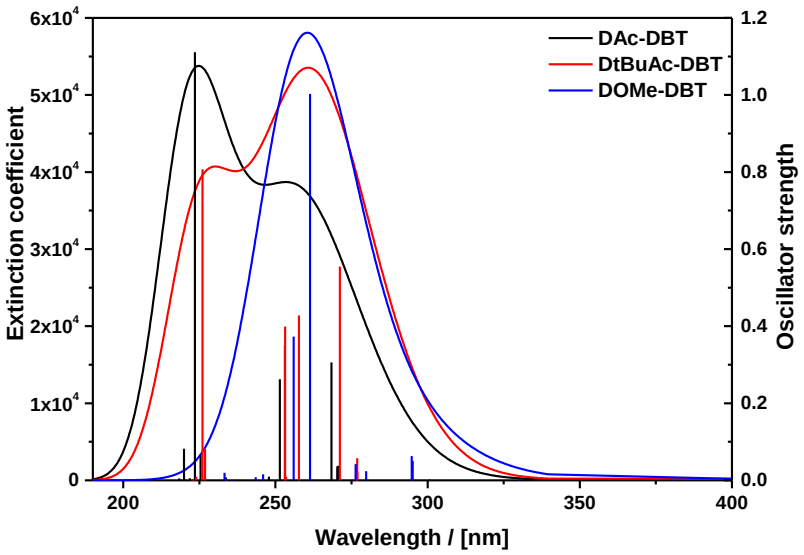

Figure S6. Theoretically predicted absorption spectra of **DAc-DBT**, **DtBuAc-DBT** and **DOMeAc-DBT** (TD-DFT rBMK/6-31G (d)).

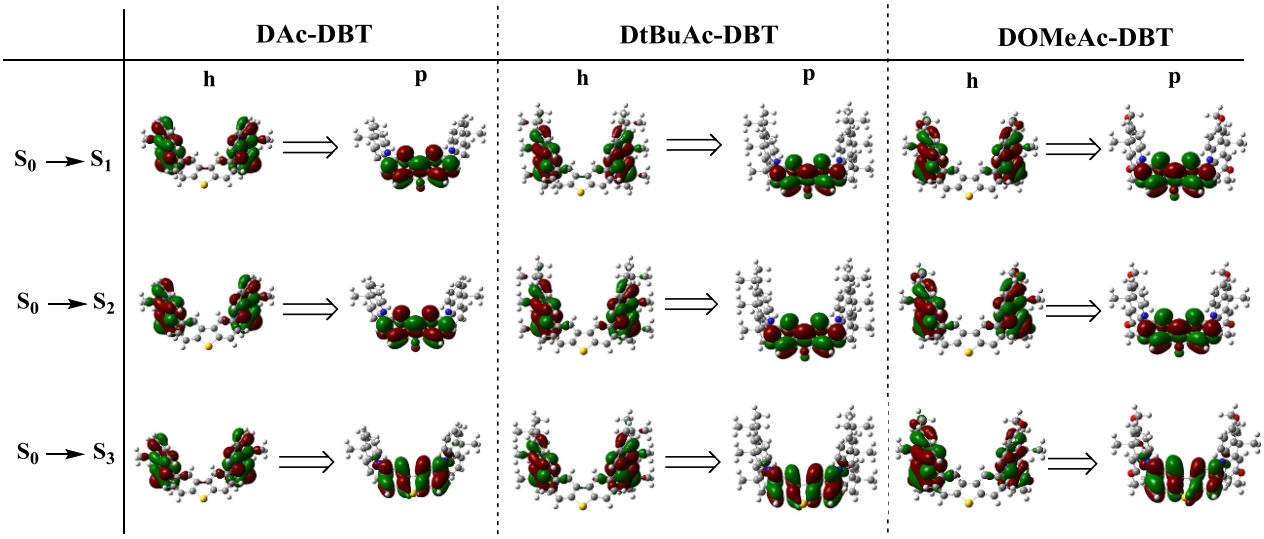

Figure S7. Natural transition orbitals (NTOs) corresponding to the first three singlet transitions in the absorption of **DAc-DBT**, **DtBuAc-DBT** and **DOMeAc-DBT** (TD-DFT rBMK/6-31G(d)).

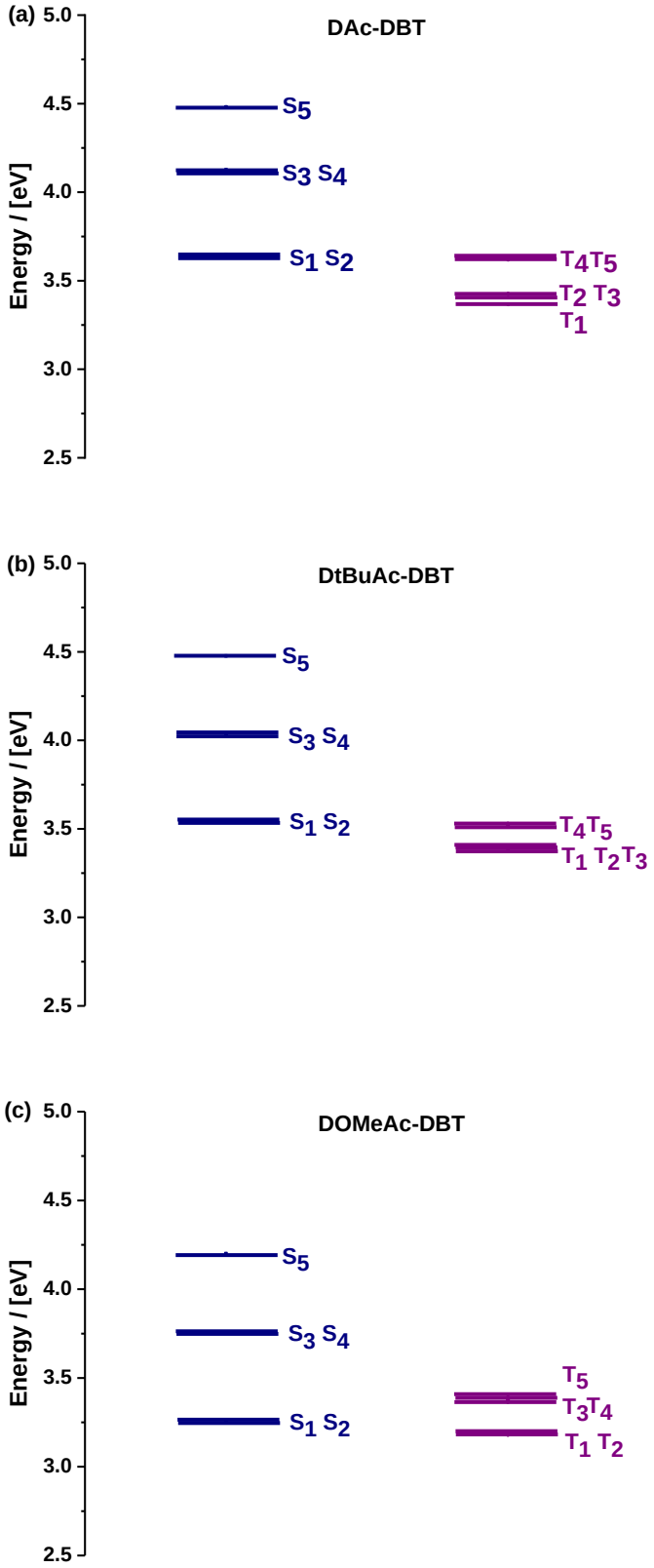

Figure S8. Singlet/triplet energy diagrams of (a) **DAc-DBT**, (b) **DtBuAc-DBT** and (c) **DOMeAc-DBT** (TD-DFT rBMK/6-31G(d)).

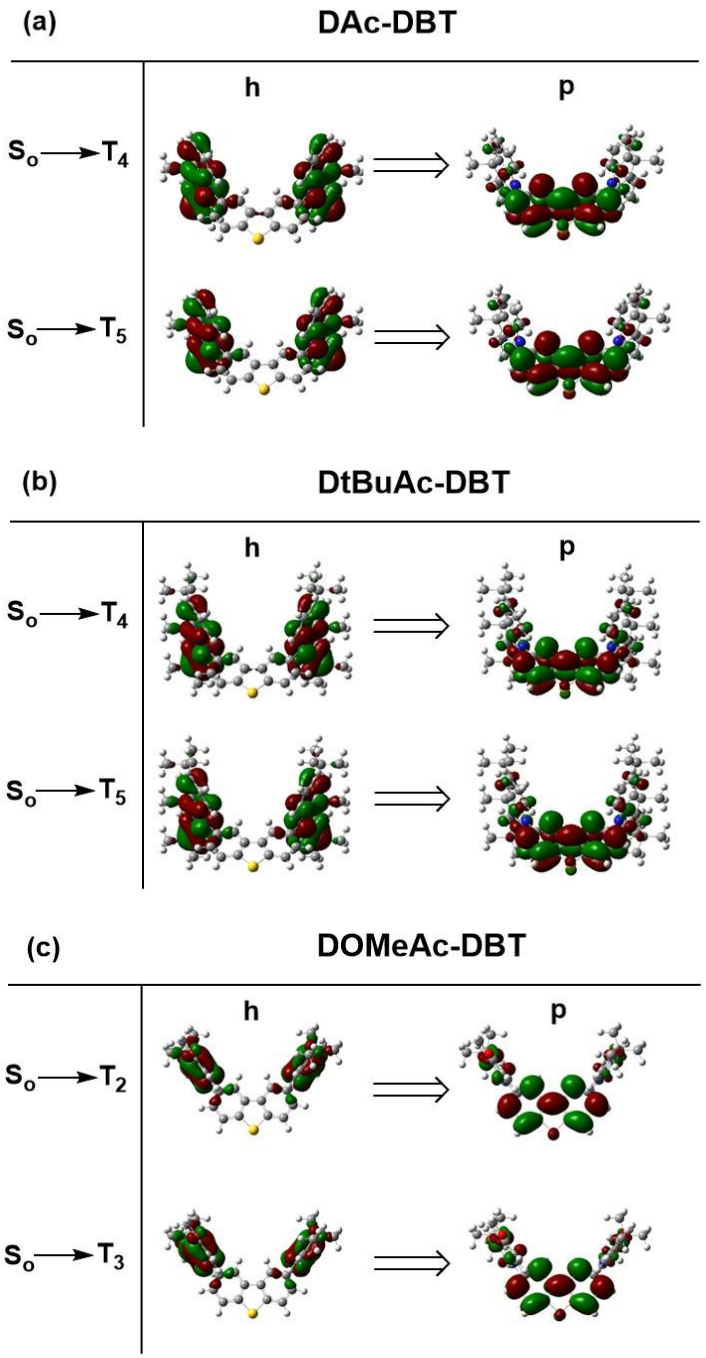

Figure S9. Selected set of natural transition orbitals (NTO) corresponding to the triplet transitions of (a) **DAc-DBT**, (b) **DtBuAc-DBT** and (c) **DOMeAc-DBT** (TD-DFT rBMK/6-31G(d)).

S4. Optical Characterization

Two types of samples were studied in this work: solutions (10^{-3} to 10^{-5} M) and films produced in zeonex matrix (1% *w/w*). All of the solutions were diluted in different solvents (ethanol, 1,2-dichlorobenzene, toluene and methylcyclohexane) and stirred for up to 24 hours. To remove oxygen for emission measurements, solutions were degassed by four freeze

–pump-thaw cycles. The films in zeonex matrix were fabricated by drop-casting onto quartz substrates. Steady-state absorption and emission spectra were acquired using a UV-3600 Shimadzu spectrophotometer and a Jobin Yvon Horiba Fluoromax 3, respectively. PLQYs were measured using a calibrated Horiba Quanta-Φ integrating sphere coupled to a Fluorolog3 spectrometer using 315 nm excitation. Data was processed using the included FluorEssence software.

Prompt fluorescence (PF), delayed fluorescence (DF) and phosphorescence spectra and time-resolved decays were recorded using nanosecond gated luminescence and lifetime measurements (from 800 ps to 1 s) with either a high energy pulsed Nd:YAG laser emitting at 355 nm (EKSPLA) and a N_2 laser emitting at 337 nm with pulse width 170 ps. Emission was focused onto a spectrograph equipped with 300 lines/mm grating of 500 nm or 1000 nm base wavelength and detected on a sensitive gated iCCD camera (Stanford Computer Optics) with sub-nanosecond resolution. Time-resolved measurements were performed by exponentially increasing the gate and delay times. The delay and integration times are chosen in a way that the next delay is set at a time longer than the previous delay+integration time. Therefore, no spectral overlap exists between the spectra corresponding to successive delays. The curve obtained directly from this process does not represent the real luminescence decay. However, this is easily corrected by integrating the measured spectra and dividing the integral by the corresponding integration time. In this way, each experimental point represents a snap-shot of the number of photons emitted per second at a time t = delay + (integration time)/2. The luminescence decay is then obtained by plotting each experimental point versus time, and fitting with sum of exponentials when required. In this way we are able to collect the entire emission spectrum decaying over 8 decades in a single experiment [13]. For initial development of these methods see previously published literature.[14]

S5. Cyclic Voltammetry Measurements

Electrochemical measurements were performed in solutions of 0.1 M Bu_4NBF_4 (99%, Sigma Aldrich, dried) in dichloromethane (DCM, 99.9%, Extra Dry, stabilized, AcroSeal®, Acros Organics) at room temperature. Solutions were prepared with 1.0 mM concentrations of the D–A–D compound and purged with nitrogen prior to measurement. The electrochemical cell is composed of three electrodes: a platinum disc with 1 mm diameter of working area as a working electrode, an Ag/AgCl electrode as a reference electrode and a platinum wire as an auxiliary electrode. All cyclic voltammetry (CV) measurements were performed at room temperature with a potential scan rate of 50 mV/s and calibrated against a ferrocene/ferrocenium (Fc/Fc^+) redox couple.

The onset potential was determined from the intersection of two tangents drawn at the rising and background current of the CV. The ionization potential (IP) was calculated from the oxidation (E_{ox}) potential, using the following equation: $IP = E_{ox} + 5.1$.[15] HOMO energy levels were determined using CV analysis by the estimation of IPs which are similar to the HOMO energies. [16] As the reduction potential is out of range even in DMF solution, LUMO energies

were calculated according to the optical band gap E_g, which was determined from the onset of the UV-Vis absorption band in DCM.

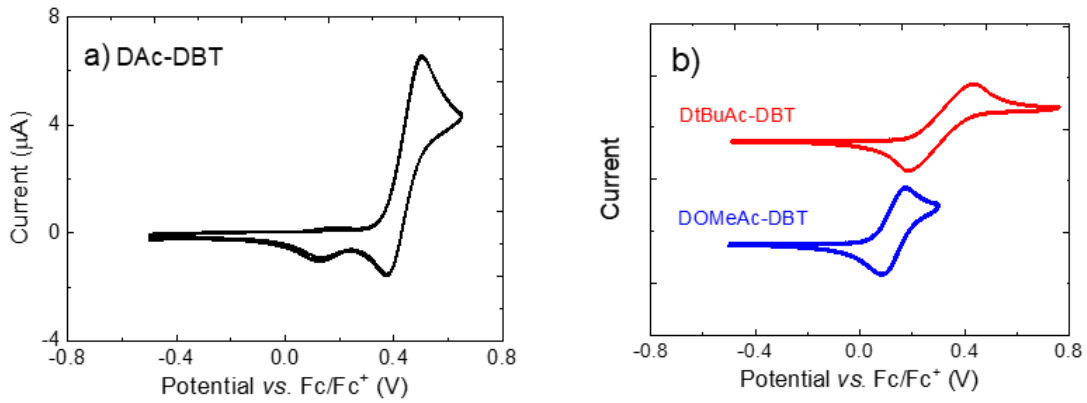

Figure S10. Cyclic voltammograms of the investigated molecules a) **DAc-DBT**, b) **DtBuAc-DBT** and **DOMeAc-DBT** at 1 mM concentration in DCM.

Table S3. HOMO and LUMO energy levels and band gaps of **DAc-DBT**, **DtBuAc-DBT** and **DOMeAc-DBT.**

Molecule	**HOMO (eV)**	**LUMO (eV)**	E_g **(eV)**
DAc-DBT	-5.45	-2.18	3.27
DtBuAc-DBT	-5.31	-2.15	3.12
DOMeAc-DBT	-5.15	-2.05	3.10

For **DAc-DBT**, a new peak is observed on the reverse scan at a lower potential resulting from degradation or reaction of the molecule leading to the formation of a conducting layer on the working electrode. This peak was not observed in the substituted derivatives **DtBuAc-DBT** and **DOMeAc-DBT** suggesting that its origin may be reactivity at the 2,7-positions of acridine. Similar behaviour was observed in other unsubstituted acridine derivatives [17] pointing to the lack of electrochemical stability. Furthermore, the HOMO energies are elevated with the increasing donor strength, which is consistent with the calculations shown in **Figure S4**. LUMO energies are determined from the HOMO levels and the corresponding optical band gaps. The HOMO and LUMO energy levels are shown in **Table S3**.

S6. Thermal properties

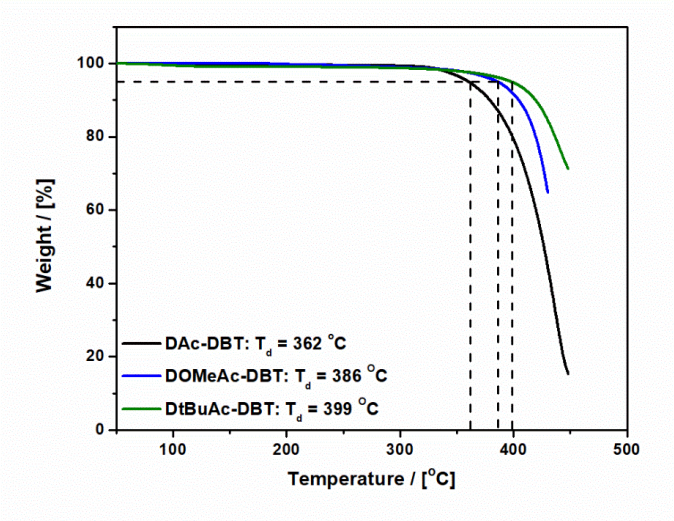

Figure S11. TGA analysis under N_2 with ramping temperature at 10 °C min^{-1} for compounds **DAc-DBT**, **DtBuAc-DBT** and **DOMeAc-DBT** with reported 5% wt. loss values.

Thermal stability of the derivatives was probed by thermal gravimetric analysis (TGA). The TGA curves along with the decomposition temperatures (T_d) at the 5% wt. loss points are presented in **Figure S11**. The T_d values increase in the sequence **DAc-DBT** < **DOMe-DBT** < **DtBuAc-DBT**. Obviously, substitution of the 2,7-positions of the acridine unit leads to an enhancement of thermal stability. **DtBuAc-DBT** exhibited the highest thermal stability owing to the presence of bulky *tert*-butyl groups.

S7. Photophysical Properties

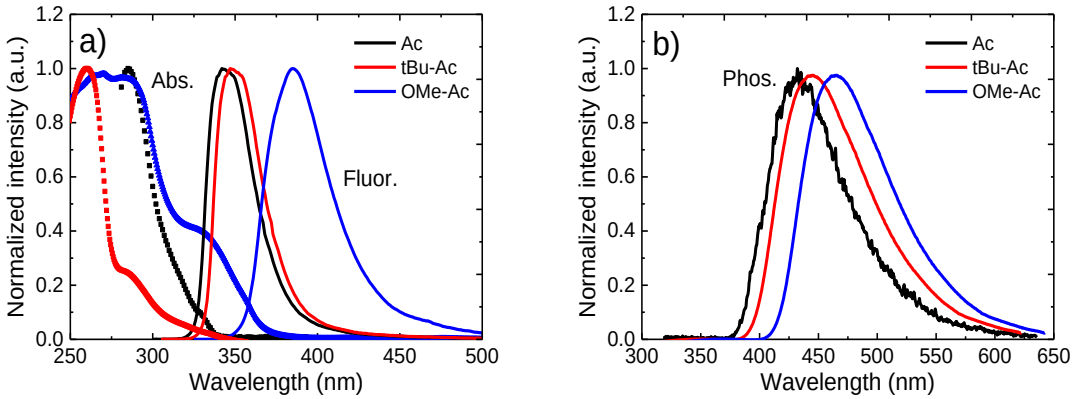

Figure S12. a) UV/Vis absorption and fluorescence spectra in toluene collected at room temperature and b) phosphorescence spectra of donor units **Ac**, **tBu-Ac** and **OMe-Ac** in zeonex recorded at 80 K.

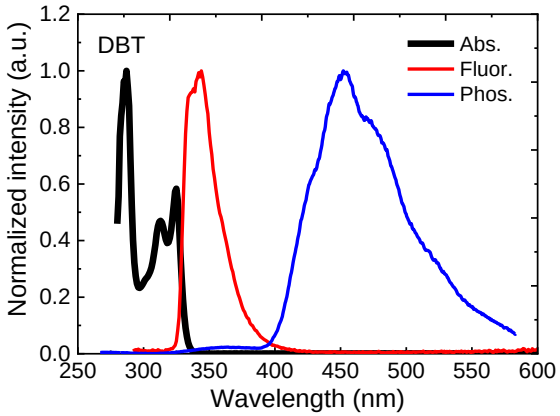

Figure S13. UV-Vis absorption (black dotted line) and fluorescence (red line) of the acceptor **DBT** unit in toluene at room temperature and phosphorescence spectra (blue line) in zeonex at 80 K.

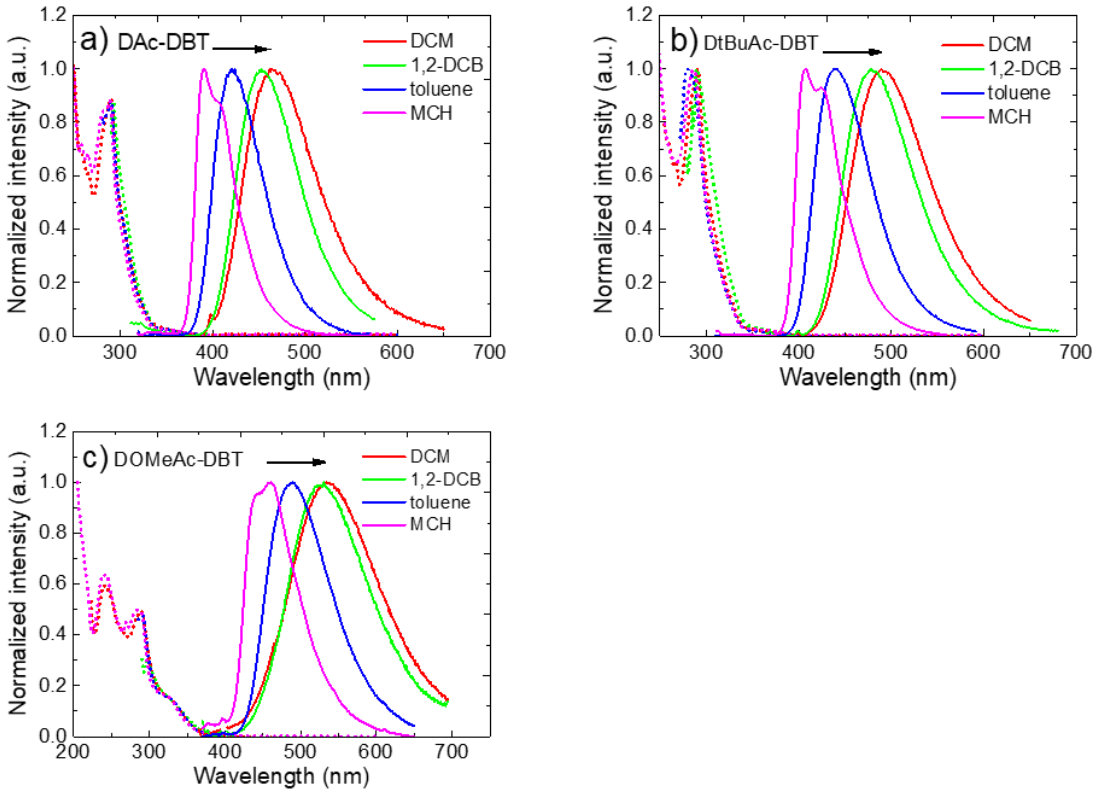

Figure S14. The normalized absorption and emission spectra in various solvents of a) **DAc-DBT**, b) **DtBuAc-DBT** and c) **DOMeAc-DBT** at room temperature.

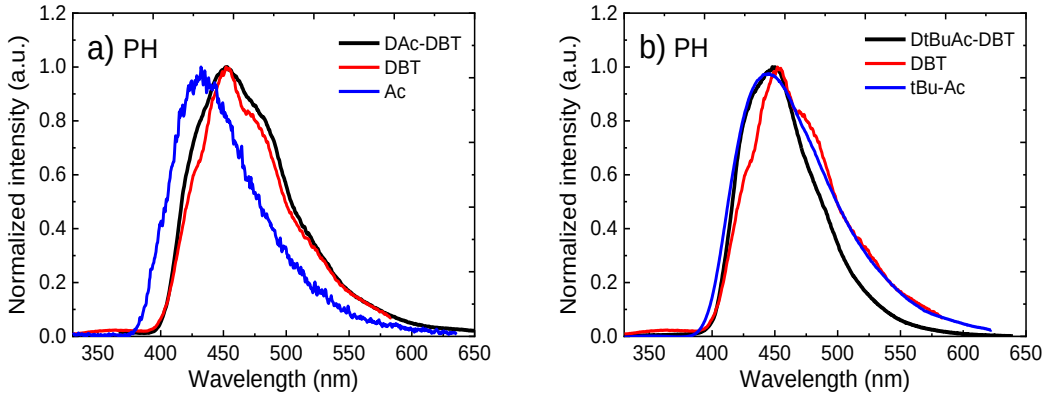

Figure S15. Phosphorescence spectra of a) **DAc-DBT** and b) **DtBuAc-DBT** in zeonex films in comparison to their individual D and A units. All spectra are measured at 80 K.

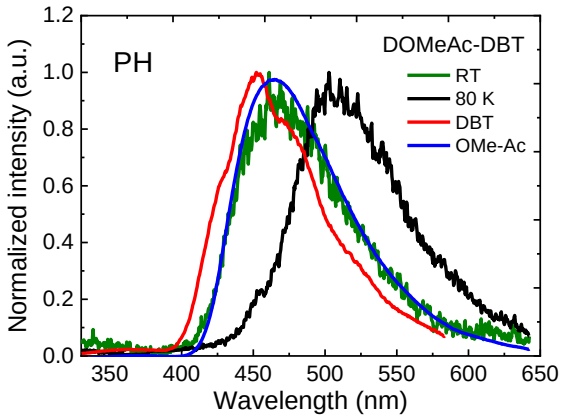

Figure S16. Phosphorescence spectra of **DOMeAc-DBT** in zeonex film measured at room temperature (dark green line) and 80 K (black line), compared with the spectra of their individual D and A units.

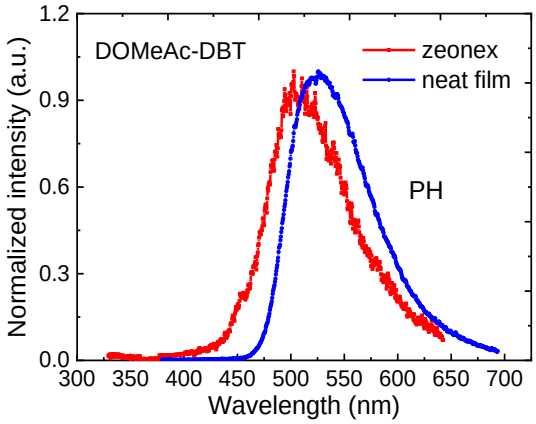

Figure S17. Phosphorescence spectra of **DOMeAc-DBT** in zeonex and neat film collected at 56 ms at 80 K. Excitation at 355 nm.

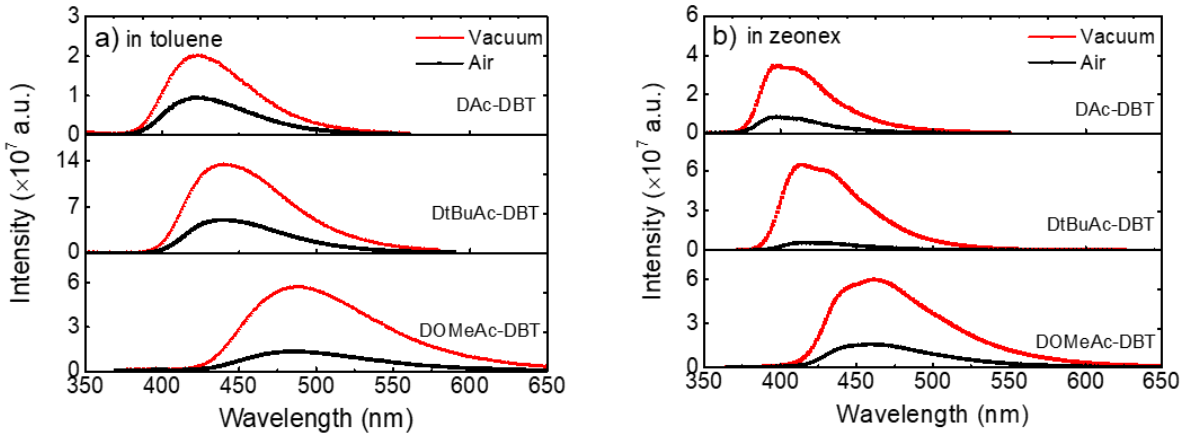

Figure S18. The steady-state emission spectra of **DAc-DBT**, **DtBuAc-DBT** and **DOMeAc-DBT** in a) diluted toluene solution (10^{-5} M) and b) zeonex films (1wt %) in the absence and presence of oxygen at room temperature, all showing that **DtBuAc-DBT** has the most efficient DF contribution.

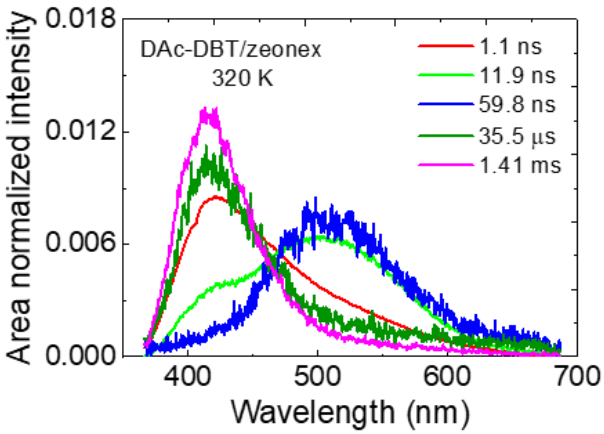

Figure S19. Time-resolved area normalized emission of **DAc-DBT** zeonex film at 320 K. Excitation at 355 nm.

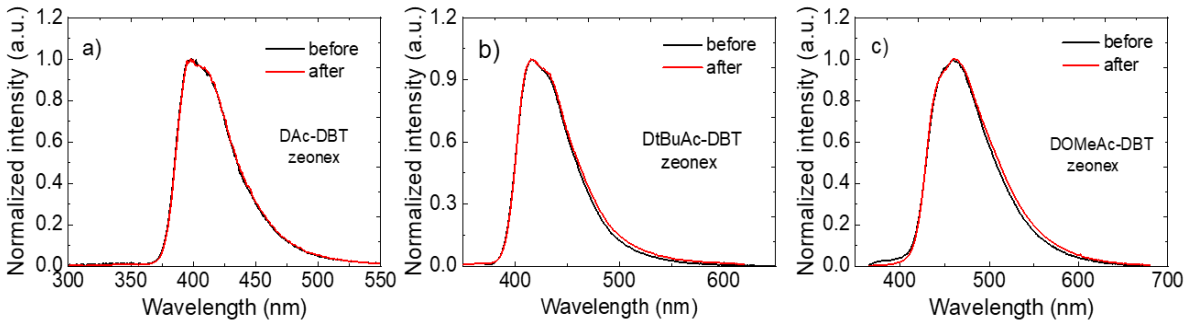

Figure S20. Steady-state emission before and after laser radiation of a) **DAc-DBT**, b) **DtBuAc-DBT** and c) **DOMeAc-DBT** in zeonex films collected at room temperature.

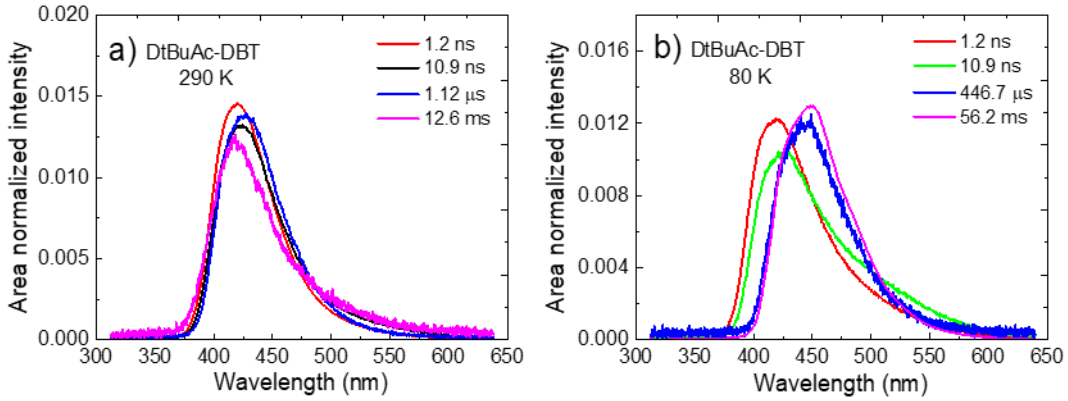

Figure S21. Time-resolved area normalized emission spectra of **DtBuAc-DBT** in zeonex matrix at a) 290 K and b) 80 K.

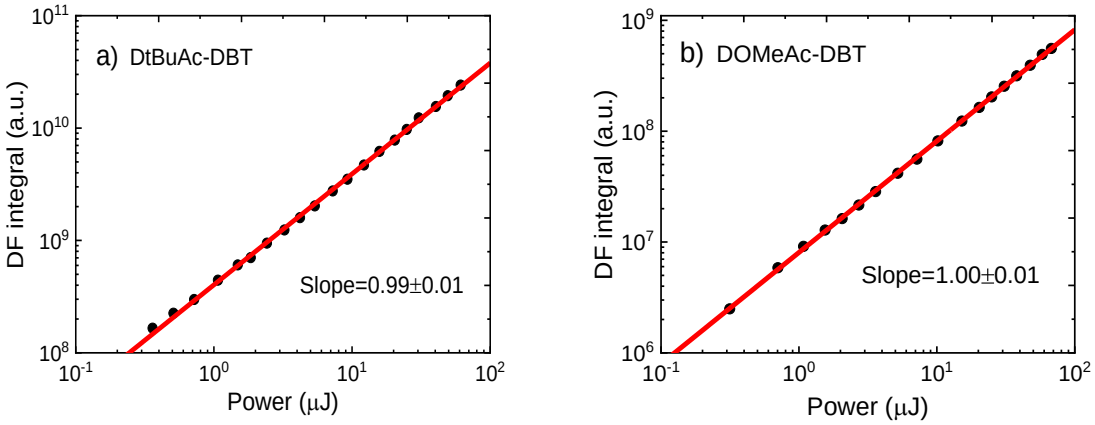

Figure S22. Power dependent measurements with delay/integration times of 1 µs/1 ms, 1 µs/200 µs for a) DtBuAc-DBT and b) DOMeAc-DBT films, respectively, excitation at 337 nm at room temperature.

S8. Devices

Organic light-emitting diodes (OLEDs) were fabricated on patterned indium-tin-oxide (ITO) coated glass (VisionTek Systems) with a sheet resisitance of 15 Ω/cm^2 using vacuum thermal evaporation. The substrates were sonicated for 15 minutes each in acetone and then IPA. After oxygen-plasma cleaning, the substrates were loaded into a Kurt J. Lesker Super Spectros 200 deposition chamber. All organic and cathode layers were thermally evaporated at a pressure below 10^{-7} mbar, at evaporation rates in the range of 0.1-0.5 A/s. The materials used for the device fabrication were: *N,N'*-bis-(naphthalene-1-yl)-*N,N'*-bis(phenyl)benzidine

(NPB) (Lumtec), 4,4-(diphenylsilanediyl)bis(*N*,*N*-diphenylaniline) (TSBPA) (Lumtec), 1,3,5-tris(*N*-phenylbenzimidazol-2-yl)benzene (TPBi) (Lumtec), bis[2-(diphenylphosphino)phenyl]ether oxide (DPEPO) (Sigma Aldrich), lithium fluoride (LiF) (99.995%, Sigma Aldrich), and aluminium (99.9995%, Alfa Aesar) were purchased from the companies.

The evaporated devices were encapsulated under inert atmosphere using UV-curable epoxy (DELO Katiobond) along the outer edges of the active emitting area with a glass coverslip. Characterization of the OLED devices was conducted in a 10-inch integrating sphere (Labsphere) coupled with a calibrated fibre spectrometer (Ocean Optics USB4000) and connected to a Keithley 2400 source measure unit.

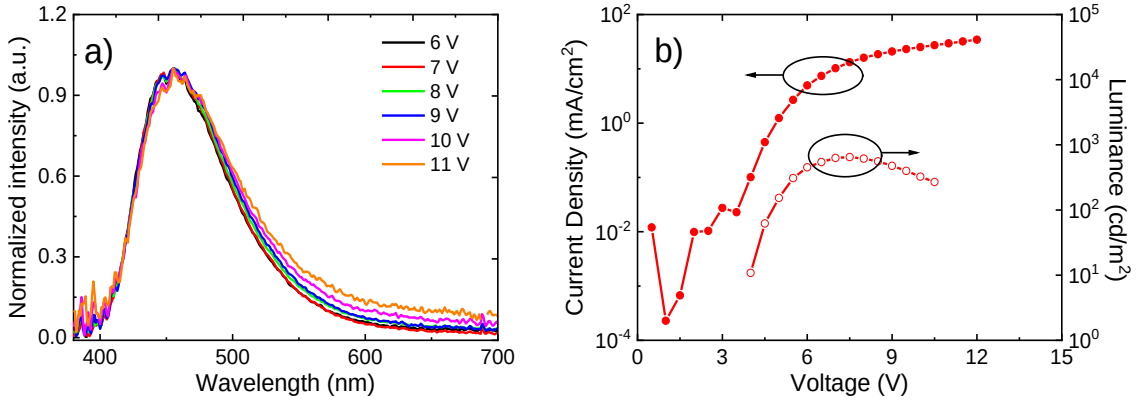

Figure S23. a) EL spectra of devices at different voltages. b) Current density-voltage-luminance (*J*-*V*-*L*) characteristics.

References

1 G. R. Fulmer, A. J. M. Miller, N. H. Sherden, H. E. Gottlieb, A. Nudelman, B. M. Stoltz, J. E. Bercaw and K. I. Goldberg, *Organometallics*, 2010, **29**, 2176–2179.

2 S. S. Reddy, V. G. Sree, K. Gunasekar, W. Cho, Y.-S. Gal, M. Song, J.-W. Kang and S.-H. Jin, *Adv. Opt. Mater.*, 2016, **4**, 1236–1246.

3 S. Kajigaeshi, T. Kakinami, H. Yamasaki, S. Fujisaki and T. Okamoto, *Bull. Chem. Soc. Jpn.*, 1988, **61**, 600–602.

4 G. M. Sheldrick, *Acta Crystallogr. Sect. A Found. Crystallogr.*, 2008, **64**, 112–122.

5 G. M. Sheldrick, *Acta Crystallogr. Sect. C Struct. Chem.*, 2015, **71**, 3–8.

6 O. V. Dolomanov, L. J. Bourhis, R. J. Gildea, J. A. K. Howard and H. Puschmann, *J. Appl. Crystallogr.*, 2009, **42**, 339–341.

7 M. J. Frisch, G. W. Trucks, H. B. Schlegel, G. E. Scuseria, M. A. Robb, J. R. Cheeseman, G. Scalmani, V. Barone, G. A. Petersson, H. Nakatsuji, X. Li, M. Caricato, A. V. Marenich, J. Bloino, B. G. Janesko, R. Gomperts, B. Mennucci, H. P.

Hratchian, J. V. Ortiz, A. F. Izmaylov, J. L. Sonnenberg, D. Williams-Young, F. Ding, F. Lipparini, F. Egidi, J. Goings, B. Peng, A. Petrone, T. Henderson, D. Ranasinghe, V. G. Zakrzewski, J. Gao, N. Rega, G. Zheng, W. Liang, M. Hada, M. Ehara, K. Toyota, R. Fukuda, J. Hasegawa, M. Ishida, T. Nakajima, Y. Honda, O. Kitao, H. Nakai, T. Vreven, K. Throssell, J. A. Montgomery, Jr., J. E. Peralta, F. Ogliaro, M. J. Bearpark, J. J. Heyd, E. N. Brothers, K. N. Kudin, V. N. Staroverov, T. A. Keith, R. Kobayashi, J. Normand, K. Raghavachari, A. P. Rendell, J. C. Burant, S. S. Iyengar, J. Tomasi, M. Cossi, J. M. Millam, M. Klene, C. Adamo, R. Cammi, J. W. Ochterski, R. L. Martin, K. Morokuma, O. Farkas, J. B. Foresman, and D. J. Fox, Gaussian, Gaussian 09, Revision A.02, *Inc., Wallingford, CT*, 2009.

8 K. S. Thanthiriwatte and S. R. Gwaltney, *J. Phys. Chem. A*, 2006, **110**, 2434–2439.

9 N. A. Kukhta, D. A. Da Silva Filho, D. Volyniuk, J. V. Grazulevicius and G. Sini, *Chem. Mater.*, 2017, **29**, 1695–1707.

10 J.-L. Brédas, *Chem. Mater.*, 2017, **29**, 477–478.

11 A. D. Boese and J. M. L. Martin, *J. Chem. Phys.*, 2004, **121**, 3405–3416.

12 T. Lu and F. Chen, *J. Comput. Chem.*, 2012, **33**, 580–592.

13 P. Pander, P. Data and F. B. Dias, *J. Vis. Exp.*, 2018, e56614.

14 C. Rothe and A. P. Monkman, *Phys. Rev. B - Condens. Matter Mater. Phys.*, 2003, **68**, 075208.

15 C. M. Cardona, W. Li, A. E. Kaifer, D. Stockdale and G. C. Bazan, *Adv. Mater.*, 2011, **23**, 2367–2371.

16 P. Data, R. Motyka, M. Lapkowski, J. Suwinski and A. P. Monkman, *J. Phys. Chem. C*, 2015, **119**, 20188–20200.

17 I. Hladka, D. Volyniuk, O. Bezvikonnyi, V. Kinzhybalo, T. J. Bednarchuk, Y. Danyliv, R. Lytvyn, A. Lazauskas and J. V. Grazulevicius, *J. Mater. Chem. C*, 2018, **6**, 13179–13189.